# Extraordinary eyes reveal hidden diversity within the holopelagic genus Paraphronima (Amphipoda: Hyperiidea)

Stenvers, Vanessa I.; Gonzalez, Brett C.; Goetz, Freya E.; Hemmi, Jan M.; Jessop, Anna Lee; Lin, Chan; Hoving, Henk Jan T.; Osborn, Karen J.

*Published in:*
Deep-Sea Research Part I: Oceanographic Research Papers

*DOI:*
10.1016/j.dsr.2021.103610



*Publication date:*
2021

Deep–Sea Research I 177 (2021) 103610

Contents lists available at ScienceDirect

Deep-Sea Research Part I

journal homepage: www.elsevier.com/locate/dsri

# Extraordinary eyes reveal hidden diversity within the holopelagic genus *Paraphronima* (Amphipoda: Hyperiidea)

Vanessa I. Stenvers [a,b,c,1,*], Brett C. Gonzalez [a], Freya E. Goetz [a], Jan M. Hemmi [d], Anna-Lee Jessop [d], Chan Lin [a], Henk-Jan T. Hoving [b], Karen J. Osborn [a,e,1]

[a] Department of Invertebrate Zoology, National Museum of Natural History, Smithsonian Institution, Washington, DC, 20013, USA
[b] GEOMAR Helmholtz Centre for Ocean Research Kiel, Düsternbrooker Weg 20, 24105, Kiel, Germany
[c] Faculty of Science and Engineering, University of Groningen, Nijenborgh 4, 9747, AG Groningen, the Netherlands
[d] School of Biological Sciences & UWA Oceans Institute, The University of Western Australia, Perth, WA, 6009, Australia
[e] Monterey Bay Aquarium Research Institute, 7700 Sandholdt Road, Moss Landing, CA, 95039-9644, USA

ARTICLE INFO

*Keywords:*
Systematics
DNA taxonomy
Micro-computed tomography (μCT)
Cryptic species
Open ocean
Midwater

ABSTRACT

Holopelagic animals were long assumed to have widespread geographic distributions due to the failure to recognize hydrographic species' barriers in the open ocean. As molecular genetic tools are more commonly used to study the ocean's inhabitants, diversity is found to be substantially higher than when inferred from morphological taxonomies alone. Here, we investigate the morphological and genetic diversity of hyperiid amphipods within the genus *Paraphronima*, currently comprising two supposedly cosmopolitan species. By combining phylogenetic analyses and four species delimitation methods (GMYC, mPTP, bPTP, ABGD), we reveal substantial species-level genetic variation. Instead of two species inhabiting multiple ocean basins, the biogeography of *Paraphronima* species appears to be limited to more regional scales. Moreover, there is morphological evidence to corroborate the observed genetic diversity. By using an integrative morpho-molecular approach, a third species from the Gulf of California, *Paraphronima robisoni* sp. nov., is described. Interestingly, the morphological characters that best distinguish the species within the genus are characters of the compound eyes, which have rarely been used for taxonomy despite being the most obvious and varied features of hyperiids. Our results warrant further investigation of presumably cosmopolitan holopelagic amphipods, while we recommend the inclusion of eye morphology in future taxonomic studies.

## 1. Introduction

The ocean's midwater zone comprises the largest and least explored habitat on the planet, stretching below the sunlit surface layer to just above the deep-sea floor. This vast habitat is characterized by an extreme physical environment (Robison, 2004, 2009), where sunlight attenuates exponentially, temperature falls to a mere 0–6°C and oxygen concentrations can reach hypoxic levels (Widder, 2002; Robison, 2004; Gilly et al., 2013). In addition, food can be hard to come by and animals have adapted to a world with little opportunity to hide (Widder, 2002; Robison, 2004). Although the open ocean is teeming with life that has evolved remarkable adaptations to deal with these prevailing conditions (Robison, 2004, 2009), most midwater animals have historically been presumed to contain limited species-level diversity. Due to the vast nature of the habitat and lack of obvious species' boundaries, species were thought to be highly connected through evolutionary time. Limited sampling and inadequate study of morphological divergence further led to the underestimation of biodiversity in the open ocean (Knowlton, 1993; France and Kocher, 1996; Norris, 2000). With the emergence of molecular genetic studies, the paradigm of cosmopolitan distributions is now slowly shifting. Biogeography of pelagic species is often restricted to smaller scales, while cryptic diversity (i.e. genetically distinct but morphologically similar) seems to be a common theme (Norris, 2000; Baird et al., 2011; Pilar Cabezas et al., 2013).

One group of animals that appears to be particularly successful in the midwater is hyperiid amphipods (Arthropoda, Malacostraca,

* Corresponding author. Department of Invertebrate Zoology, Smithsonian National Museum of Natural History, PO Box 37012 NMNH MRC 163, Washington, DC, 20013-7012, USA.
*E-mail address:* stenversve@si.edu (V.I. Stenvers).
[1] only V. I. Stenvers and K. J. Osborn are authoring the species description included in the manuscript.

https://doi.org/10.1016/j.dsr.2021.103610
Received 2 May 2021; Received in revised form 29 July 2021; Accepted 5 August 2021
Available online 8 August 2021

Peracarida). Hyperiids are among the most abundant crustacean zooplankton and an important food source for commercially important fishes (Bowman and Gruner, 1973; Vinogradov et al., 1996; Pinnegar et al., 2015). They are found circumglobally and currently consist of approximately 280 described species. In spite of their ecological significance, phylogenetic relationships within the suborder have not been fully resolved. Morphological systematics, for instance, is hampered by homoplastic characters, while limited molecular data has only recently shed light on broader phylogenetic relationships (Browne et al., 2007; Hurt et al., 2013; Copilaş-Ciocianu et al., 2020). As such, relationships among and within hyperiidean genera remain largely uncharacterized. The few studies that provide evidence of genetic diversity in single hyperiid species suggested the presence of hidden genetic complexity. These studies, however, were only based on a handful of specimens per species and did not address the variation directly (Browne et al., 2007; Tempestini et al., 2017). Intriguingly, the most obvious morphological variation that is found in hyperiids – the surprisingly broad array of compound eye designs – have seldom been used for taxonomy (Zeidler and Browne, 2015). Eye configurations in hyperiids can range from an absence of eyes, to eyes so large that they account for as much as 35% of body size (Baldwin Fergus et al., 2015). These eyes are presumably adapted to ambient light conditions and their owner's habits (Meyer--Rochow, 1978; Land, 1989), resulting in eyes that are both inconspicuous to predators and sensitive enough to locate prey.

An example of a hyperiidean genus that is characterized by highly unusual eyes and currently contains two presumably cosmopolitan species is *Paraphronima* Claus, 1879. In *Paraphronima*, the paired apposition compound eyes each have a dorsally and a laterally facing portion, and together these occupy most of the cephalon (Baldwin Fergus et al., 2015). This dual-purpose eye design is common in midwater animals (e.g. fish, crustaceans, and mollusks; Land, 2000), yet in *Paraphronima* this configuration is taken to the extreme. Instead of two viewing areas accompanied by a differentiated retina or two separated retinas within an eye, *Paraphronima* possess 12 distinct retinas within each eye. Baldwin Fergus et al. (2015) showed that each of these retinas connect to select groups of ommatidia in *Paraphronima gracilis* Claus, 1879, which are either directed upward or lateral/downward depending on their position on the eye. Each ommatidium consists of a crystalline cone and photosensing cells that form the rhabdom. The presumed function of these eyes is to detect overhead contours against the dimly lit background, while having a broad peripheral view of bioluminescent sources (Baldwin Fergus et al., 2015). It is not known how the specific arrangement of retinas or ommatidia within each eye differs between *Paraphronima* species.

Although the unique eyes in *Paraphronima* make it easy to differentiate the genus, species within the genus have proven difficult to separate (Zeidler, 2003). Not only are the two recognized species, *Paraphronima gracilis* and *Paraphronima crassipes* Claus, 1879, frequently mistaken for each other, misinterpretation of morphological variation within the group led to the proposal of six additional species between 1836 and 1888 (Guérin-Méneville, 1836; Bovallius, 1885, 1887; Stebbing, 1888). Even though Bovallius (1885) described most of these, the author later recognized that at least three should be rejected based on the discovery of sexual dimorphism and adult versus juvenile characters. One of these questionable descriptions actually belonged to the genus *Dairella* Bovallius, 1887 (Bovallius, 1889). Bovallius (1889) also noted that some of the species might be considered varieties, further indicating the difficulties of *Paraphronima* species classification.

No studies have investigated the phylogenetic relationships or genetic variation within *Paraphronima*. Broader Hyperiidea studies using molecular data have only ever included a single representative of *Paraphronima*, resulting in the move from its original placement within the Vibilioidea (Physocephalata) to sister to *Cystisoma* Guérin-Méneville, 1836, which in turn was recovered within or sister to the Physosomata (Browne et al., 2007; Hurt et al., 2013; Copilaş-Ciocianu et al., 2020). The original placement within Vibilioidea was solely based on the shape and placement of the first antennae (Bowman and Gruner, 1973). The lack of genetic data and the seemingly high level of morphological variation emphasize the phylogenetic uncertainty surrounding *Paraphronima* and highlight the need for further investigation.

The aim of this study was threefold, (*i*) to assess the genetic diversity within *Paraphronima*, (*ii*) describe a new, morphologically and genetically distinct species from the Gulf of California, México, and (*iii*) to investigate the usefulness of eye characters for taxonomy.

## 2. Materials and methods

### 2.1. Specimen collection

One holotype and thirteen paratypes of the new species, *Paraphronima robisoni* sp. nov., were collected by KJO in the Gulf of California, México from the R/V *Western Flyer* between February 22 and March 1, 2015 (Table 1). To investigate phylogenetic relationships, 67 additional specimens of *Paraphronima* were collected from the Northeast Pacific Ocean (Gulf of California and Monterey Bay) and from the North Atlantic Ocean (Florida region of the Gulf Stream and Cabo Verde) between February 22, 2015 and February 22, 2019 (Table S1, Fig. 1). Specimens from the Gulf of California and Northeast Pacific were collected with a tucker trawl net (1.5 m opening, 500 μm mesh), while those from the Gulf Stream were collected with a plankton net (1 m opening, 500 μm mesh). Specimens from Cabo Verde were collected using either the Hydrobios© Midi (0.25 $m^2$ opening, 200 μm mesh) and Maxi (0.5 $m^2$ opening, 2 mm mesh) multinets (Hoving et al., 2018, 2019) or with the suction sampler or sampling cylinders of the manned submersible JAGO (GEOMAR Helmholtz-Zentrum für Ozeanforschung et al., 2017). Cabo Verde has not ratified the Nagoya protocol. To fulfill the national ABS regulations of Cabo Verde, we obtained the required permit for sample collection in Cabo Verde waters and publication of the results from the Direcção Nacional do Ambiente (National Directorate for the Environment of Cabo Verde). All specimens were preserved in 95% ethanol or 4% formalin. Select specimens were photographed prior to preservation aboard the ship using a Canon EOS 5DSR camera with a 65 mm f/2.8 1–5x macro lens. In the laboratory, additional photographs were taken of the preserved specimens to create line drawings, and a dissecting microscope was used to verify morphological details (see Fig. S1 for terms of basic amphipod anatomy and abbreviations).

For the outgroups, two taxa were collected from the same cruise as the *P. robisoni* sp. nov. specimens in order to represent the old and new phylogenetic position of *Paraphronima* (i.e. Vibilioidea vs. Physosomata, respectively), including *Vibilia* sp. Milne Edwards, 1830 and *Scypholanceola aestiva* (Stebbing, 1888).

The type series of *P. robisoni* sp. nov (Table 1). was compared to the type descriptions of *P. gracilis* and *P. crassipes* in addition to the descriptions of the unaccepted *Paraphronima* species proposed by Guérin-Méneville (1836), Bovallius (1885, 1887) and Stebbing (1888). Moreover, all *P. crassipes* (due to their close likeness to *P. robisoni* sp. nov.) and select *P. gracilis* samples at the Smithsonian National Museum of Natural History (USNM) were examined in the light of our discovery that there are more than two *Paraphronima* species.

### 2.2. DNA extraction and sequencing

DNA was extracted from dissected legs or from whole specimens using the automated AutoGenprep965 (AutoGen, Inc., Holliston, MA) and the proteinase K/phenol extraction method following the manufacturer's tissue protocol. Partial sequences of the nuclear 18S rRNA (V1-2 region), 16S rRNA and mitochondrial COI genes were amplified. Polymerase chain reactions (PCR) were performed in 10 μL volumes for each of these markers, containing 5.95 μL $ddH_2O$, 1.0 μL 10X Buffer, 0.6 μL $MgCl_2$ (50 mM stock), 0.5 μL dNTPs (10 mM stock), 0.25 μL BSA (10 mg/μL stock), 0.3 μL for both forward and reverse primers (10 μM stock), 0.1 μL Bioline Taq (5 Units/μL stock) and 1.0 μL DNA template.

**Table 1**
*Paraphronima robisoni* sp. nov. types.

| Date | Location | USNM # | Preservative | Collection depth (m) | Sex | Fate |
|---|---|---|---|---|---|---|
| 22 Feb 15 | 24.278°N 109.360 °W | 1290934 | 95% Ethanol | 200–700 | Juvenile | Paratype (DNA extract) |
| 23 Feb 15 | 24.310°N 109.213°W | 1290989 | 95% Ethanol | 800–1600 | Female | Paratype (DNA extract) |
| 25 Feb 15 | 25.4417°N 109.848°W | 1291026 | 95% Ethanol | 25–856 | Female | Holotype |
| 25 Feb 15 | 25.4417°N 109.848°W | 1615585 | 95% Ethanol | 25–856 | Male | Paratype (MicroCT) |
| 25 Feb 15 | 25.4417°N 109.848°W | 1617014 | 95% Ethanol | 25–856 | Male | Paratype |
| 25 Feb 15 | 25.4417°N 109.848°W | 1617015 | 95% Ethanol | 25–856 | Male | Paratype |
| 25 Feb 15 | 25.4417°N 109.848°W | 1617016 | 95% Ethanol | 25–856 | Male | Paratype (DNA extract) |
| 28 Feb 15 | 25.440°N 109.852°W | 1253893 | Formalin | 20–739 | Female | Paratype (DNA extract) |
| 28 Feb 15 | 25.440°N 109.852°W | 1253894 | Formalin | 20–739 | Female | Paratype (DNA extract) |
| 28 Feb 15 | 25.440°N 109.852°W | 1253892–1 | Formalin | 20–739 | Female | Paratype |
| 28 Feb 15 | 25.440°N 109.852°W | 1253892–2 | Formalin | 20–739 | Female | Paratype |
| 01 Mar 15 | 24.310°N 109.213°W | 1253946–1 | Formalin | 20–1555 | Female | Paratype |
| 01 Mar 15 | 24.310°N 109.213°W | 1253946–2 | Formalin | 20–1555 | Female | Paratype |
| 01 Mar 15 | 24.310°N 109.213°W | 1253946–3 | Formalin | 20–1555 | Female | Paratype |

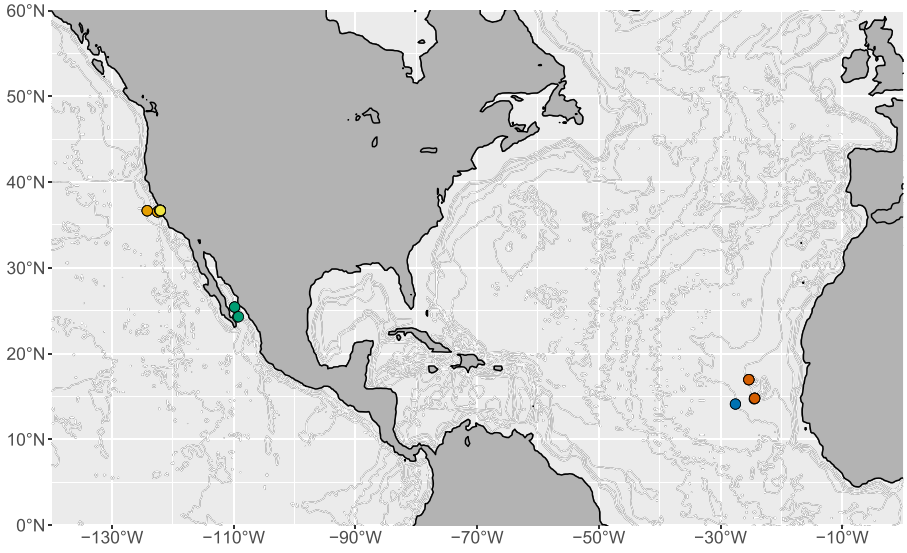


**Fig. 1.** Geographic distribution of genetic samples of *Paraphronima robisoni* sp. nov. (green), *Paraphronima* cf. *gracilis* (yellow), *Paraphronima* cf. *crassipes* (blue), *Paraphronima* sp. A (red) and *Paraphronima* sp. B (orange). (For interpretation of the references to colour in this figure legend, the reader is referred to the Web version of this article.)

An approximate 460 bp fragment of the 18S V1-2 region was obtained using the primers 18S-SSU-F04 5′-GCT TGT CTC AAA GAT TAA GCC-3′ and 18S-SSU-R22 5′-GCC TGC TGC CTT CCT TGG A-3’ (Blaxter et al., 1998). The thermocycling conditions were 2 min denaturation at 95°C, followed by 35 cycles of 95°C for 60 s, 57°C for 45 s, 72°C for 180 s, and a final extension of 72°C for 10 min. The 16S amplicon was ~450 bp using primers 16 Sar 5′-CGC CTG TTT ATC AAA AAC AT-3′ and 16Sbr 5′-CCG GTC TGA ACT CAG ATC ACG T-3’ (Palumbi, 1996). The thermocycling protocol for these primers had to be optimized to increase amplification success and resulted in the following program: 3 min denaturation at 94°C, followed by a touchdown for 5 cycles of 94°C for 30 s, 43°C for 30 s and 68°C for 45 s, followed by another 35 cycles at 94°C for 30 s, 49°C for 30 s, 68°C for 45 s and a final extension at 72°C for 5 min. To obtain the ~658 bp sequence of COI, the degenerate primers jgLCO1490 5′-TIT CIA CIA AYC AYA ARG AYA TTG G-3′ and jgHCO2198 5′-TAI ACY TCI GGR TGI CCR AAR AAY CA-3’ (Geller et al., 2013) were used. The thermocycling conditions were as follows: 7 min denaturation at 95°C, followed by 40 cycles at 95°C for 45 s, 42°C for 45 s and 72°C for 60 s, with a final extension at 72°C for 5 min.

To test the success of the amplification, 1.8 μL of PCR product was loaded on a 1.5% agarose/SB-buffer (Sodium hydroxide-Boric Acid buffer) gel together with 2 μL of a 1.5:1000 dilution of GelRed® (Biotium). After verification, PCR products were cleaned by adding 0.5 μL ExoSAP-IT™ (ThermoFisher Scientific) and 1.5 μL of $ddH_2O$ to each sample followed by thermocycling for 30 min at 37°C and 20 min at 80°C with a final hold at 12°C. Cycle sequencing reactions were carried out using 1 μL of cleaned PCR product and 9 μL of master mix containing 6.25 μL $ddH_2O$, 1.75 μL 5x Buffer, 0.5 μL of each primer and 0.5 μL BigDye® Terminater v3.1 (Applied Biosystems). The thermocycling protocol for sequencing consisted of 30 cycles at 95°C for 30 s, 50°C for 30 s and 60°C for 4 min, with a final hold at 12°C. All products were purified using Sephadex™ G-50 Fine (GE Healthcare) gel column filtration, after which they were bidirectionally sequenced on an ABI 3730 DNA Analyzer (Applied Biosystems, Foster City, CA, USA).

All sequences were assembled and cleaned using Geneious Prime 2020.1.1 (Biomatters, Auckland, New Zealand) and aligned with the Geneious MAFFT plugin (Katoh and Standley, 2013). All generated sequences were deposited in GenBank under the accession numbers MW405576–MW405619, MW404102–MW404152 and MW404044 –MW404101 (Table S1).

### 2.3. Phylogenetic analyses

In addition to sampled specimens, two *Paraphronima* (HM053501,

EF989674) and one *Vibilia cultripes* Vosseler, 1901 (KF430277) sequences were obtained from the GenBank database and added to the dataset. Phylogenetic reconstructions were performed on individual and concatenated (18S + 16S + COI) gene datasets using methods of maximum likelihood (ML) and Bayesian Inference (BI) as implemented on the CIPRES Science Gateway (Miller et al., 2010). The ML analysis was performed in RaxML 8.2.12 (Stamatakis, 2014), which only implements general time reversible (GTR) models of sequence evolution for amino acids. As such, a GTR model with corrections for discrete gamma distribution (GTR+Γ) was specified. Non-parametric bootstrapping with 1000 replicates was used to generate nodal support estimations.

Before executing the BI analysis, jModelTest2 (Darriba et al., 2012) was used to estimate the best evolutionary model based on the corrected Akaike Information Criterion (AICc). These models included a symmetrical model with gamma distribution (SYM +Γ) for 18S rRNA, a generalized time reversible with gamma distribution (GTR+Γ) for 16S rRNA and a GTR model with gamma distribution and invariable sites (GTR + I+Γ) for COI. Bayesian analyses were performed using MrBayes 3.2.7a (Ronquist et al., 2012) as implemented on the CIPRES Science Gateway. Both individual and concatenated gene datasets were run with two independent analyses using four chains (three heated, one cold) for 30 million generations with a sampling every 1000 generations. Burnin length was set to 10 million generations. Majority-rule consensus trees (50%), posterior probabilities and branch lengths were reconstructed using the trees remaining after burnin. Convergence of all MCMC runs were checked using Tracer v1.7.1 (Rambaut et al., 2018).

### 2.4. Species delimitation

Genetic divergence was investigated for single and concatenated gene sets (including COI, 16S, COI+16S, COI+18S, 16S + 18S and COI+16S + 18S) using four widely accepted species delimitation methods (Fontaneto et al., 2015). These included the generalized mixed Yule-coalescent (GMYC) model (Fujisawa and Barraclough, 2013), the multi-rate Poisson tree process (mPTP; Kapli et al., 2017), the Bayesian implementation of Poisson tree process (bPTP; Zhang et al., 2013) and the Automatic Barcode Gap Discovery (ABGD) model (Puillandre et al., 2012). Both GMYC and PTP analyses were performed on ultrametric gene trees (described below), which we generated using BEAST v1.10.4 (Drummond et al., 2012) as implemented on the CIPRES Science Gateway (Miller et al., 2010). Since BEAST does not rely on branch smoothing, this method is known to provide the most robust and consistent estimates of evolutionarily significant units (Tang et al., 2014). Since both mPTP and bPTP methods can also utilize non-ultrametric gene trees, we additionally ran our PTP analyses using the ML trees constructed with RAxML (as described above) to assess model robustness. GMYC analyses were carried out in R v3.5.2 (R Core Team, 2017) with the package SPLITS v1.0-19 (Ezard et al., 2009). The PTP models were analyzed on the mPTP online server (https://mptp.h-its.org) with default settings and on the bPTP server (https://species.h-its.org) with 100,000 MCMC generations and 0.1 burnin.

To compare the above-mentioned tree-based methods, the ABGD model was calculated based on genetic pairwise distances. Where tree-based methods heavily rely on the monophyly of species clades to delimitate species, the ABGD method will also recognize para- and polyphyletic species boundaries (Fontaneto et al., 2015). This model assumes intraspecific variation to be lower than interspecific distances and uses these 'barcode gaps' (i.e. greater pairwise differences) to separate taxonomic units. The ABGD model was carried out on the online platform (https://bioinfo.mnhn.fr/abi/public/abgd/abgdweb.html) using default parameters. Prior to all delineation analyses, identical sequences with zero genetic distance were removed from the datasets. Genetic distances were calculated with MEGA X (Kumar et al., 2018) using the Kimomura 2-parameter model and setting the variation among sites to gamma distributed rates (parameter 1), eliminating missing base pair positions. Outgroups were also removed in all four delimitation methods.

The Bayesian Evolutionary Analysis Utility (BEAUti) v1.10.4 was used to create XML files for BEAST runs. Two separate analyses were run to compare different tree priors, including the Yule Process and Coalescent model with constant population size. The rate of molecular evolution was set to a strict clock, which is considered the most suitable clock for related species with low levels of rate variation between branches (Brown and Yang, 2011). The nucleotide substitution model was determined with help of the AICc in jModelTest2 (Darriba et al., 2012) and resulted in a Hasegawa, Kishino and Yano model with gamma distribution (HKY+Γ) for 18S rRNA, a generalized time reversible with gamma distribution (GTR+Γ) for 16S rRNA and a GTR model with gamma distribution and invariable sites (GTR + I+Γ) for COI. All runs were set to 100 million generations, sampling trees every 10,000 generations. Convergence of the MCMC runs was evaluated using Tracer v1.7.1 (Rambaut et al., 2018). A maximum clade credibility (MCC) consensus tree for each run was generated in TreeAnnotator v1.10.4 by analyzing the remaining 9001 trees after burn-in.

### 2.5. Eye morphology

To investigate differences in eye morphology, one of the *P. robisoni* sp. nov. paratypes ($n_{eyes} = 2$), one *P.* cf. *crassipes* ($n_{eyes} = 2$), two *P.* cf. *gracilis* ($n_{eyes} = 4$) and four *Paraphronima* sp. A ($n_{eyes} = 8$) were analyzed using micro-computed tomography (microCT). Before the microCT scans, specimens were stained with 0.5–0.6% Phosphotungstic acid and 3% Dimethylsulfoxide in 70% ethanol or with 1% iodine in 100% ethanol for a variable number of days (see Table S2). Specimens were then mounted in a 200 μL pipette tip with 0.5% low melt agarose mixed with reverse osmosis water. The pipette tip was melted to seal the small end and the wide end coated in paraffin to prevent evaporation. The specimens were microCT scanned with the GE Phoenix v|tome|x M 180 kV Nano Tube at the Smithsonian National Museum of Natural History Scientific Imaging facility. For settings of the microCT scanner in voltage, current, power, voxel size and exposure time, see Table S2. In the scanned *P. robisoni* sp. nov. paratype (USNM1615585), the ischium to dactylus of the left fifth pereopod was lost and are therefore absent from the microCT body scan (Fig. 6A). MicroCT scans were analyzed with custom MATLAB 2019b (The MathWorks Inc.) software (Bagheri et al., 2020) and DragonFly 2020.2 (Object Research Systems Inc.). The images in Fig. 6 were constructed in Amira 2020.2 (ThermoFisher Scientific).

## 3. Results

### 3.1. Phylogenetic analyses

Based on the phylogenetic analyses, a new species from the Gulf of California, México was identified and named *Paraphronima robisoni* sp. nov., for which the species description and morphological divergence will be discussed shortly (sections 3.3–3.13). The maximum likelihood (ML) and Bayesian Inference (BI) analyses produced nearly identical tree topologies for each of the individual genes and for the concatenated gene dataset. Therefore, only BI trees are shown with ML support values added (Fig. 2). There were differences and similarities in the estimated topologies for each gene that reflect the difference in divergence rate within each marker. Both COI and 16S returned well-supported clades for *P. robisoni* sp. nov. (1.0 pp and 82/100 bs), sister to an additional *Paraphronima* clade referred to here as *Paraphronima* sp. A (1.0 pp and 98/99 bs; Fig. 2A and B). In addition, COI and 16S returned a well-supported clade (1.0 pp and 100 bs) that we, for now, interpret as *P.* cf. *crassipes* based on both these specimens' agreement with the description and collection range originally reported for *P. crassipes* (Claus, 1879; i.e. Atlantic Ocean and Mediterranean Sea). *Paraphronima* cf. *gracilis* was recovered sister to the remaining *Paraphronima* clades for

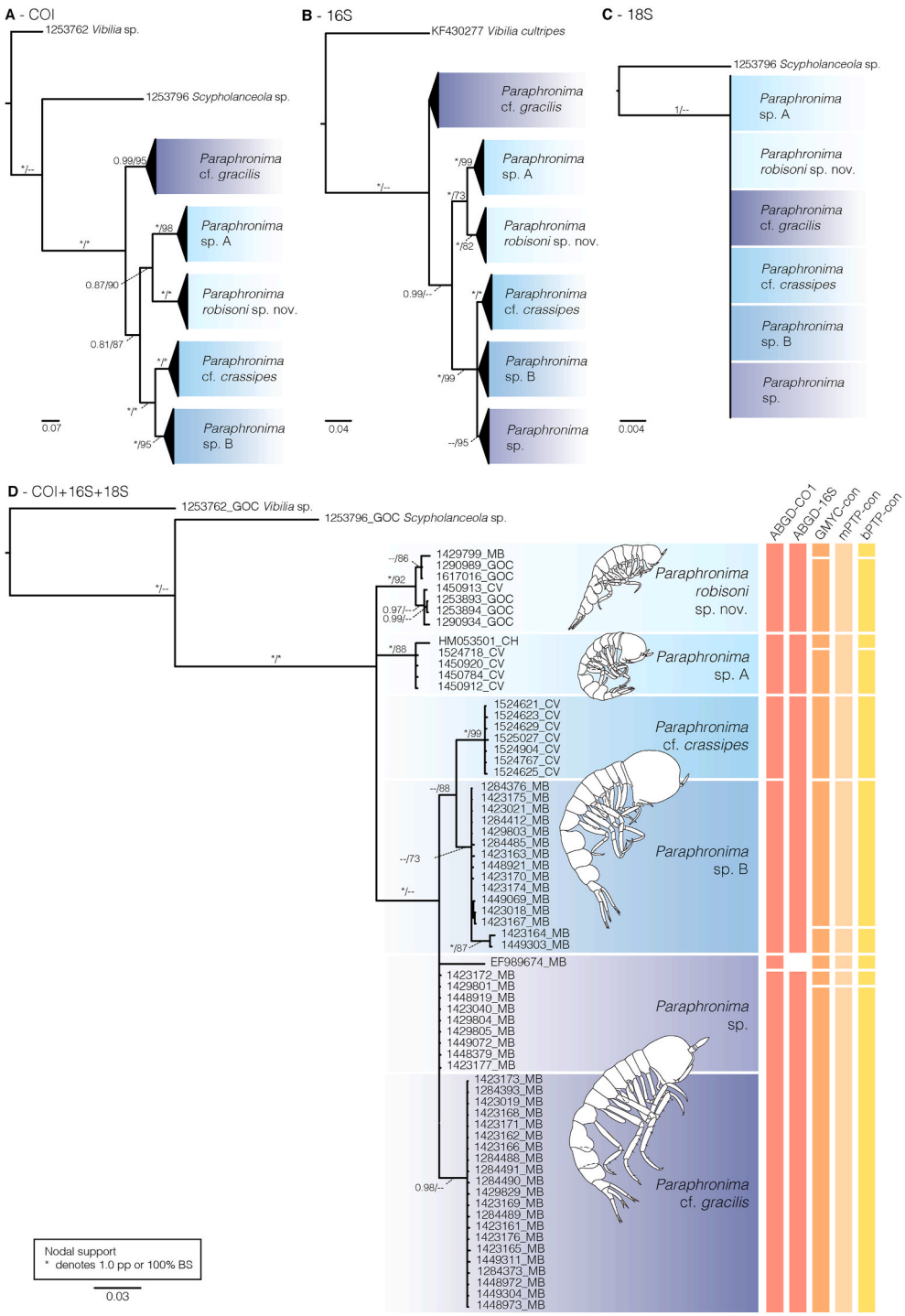


**Fig. 2.** Bayesian Inference phylogenies of *Paraphronima* with support values from maximum likelihood (ML) analyses provided, showing single gene trees for the (A) COI, (B) 16S rRNA (C) 18S rRNA, and (D) concatenated dataset of all three genes. Support shown as Bayesian posterior probabilities (PP)/ML bootstrap (BS) values. Support below 0.95 pp or 70% bs and nodes not present in the corresponding analysis are indicated with a dash. Cool colour blocks indicate the five recovered clades and polyomous *Paraphronima* sp. specimens. Letters following the specimen numbers indicate geographic locality, including Gulf of California (GOC), Monterey Bay (MB), Cabo Verde (CV) and China (CH). Results of the four species delimitation methods are indicated by vertical bars, including the Automated Barcode Gap Discovery (ABGD for COI and 16S rRNA), and for the concatenated (con) dataset using the Generalized Mixed Yule-Coalescent (GMYC) model, the multirate Poisson Tree Process (mPTP) and the Bayesian implementation of Poisson Tree Process (bPTP). Breaks between bars indicate most conservative estimates of species boundaries. (For interpretation of the references to colour in this figure legend, the reader is referred to the Web version of this article.)

COI (0.99 pp and 95 bs; Fig. 2A), while in 16S, sequences appeared to be split between two weakly supported clades – including a clade identified as *P.* cf. *gracilis* and a clade herein referred to as *Paraphronima* sp. (Fig. 2B). It is possible that these *Paraphronima* sp. specimens show similarity to *P.* cf. *gracilis*, as one of them (USNM1423172) clustered with high support within the COI *P.* cf. *gracilis* clade. COI and 16S differed in their support for the specimens identified as *Paraphronima* sp. B, which were sister to *P.* cf. *crassipes* in COI (1.0 pp and 95 bs) but emerged from a polytomy next to *P.* cf. *crassipes* and *Paraphronima* sp. in 16S (Fig. 2B). The short region of 18S had too little variation to resolve any clade other than *Paraphronima* and even that was unsupported in the ML analysis (Fig. 2C).

The concatenated analysis similarly recovered the five clades from the COI tree, though with weak support for *Paraphronima* sp. B (0.89 pp and 73 bs) and *P.* cf. *gracilis* (0.98 pp and 64 bs) in the BI and ML analyses, respectively (Fig. 2D). Specimens of *Paraphronima robisoni* sp. nov. were recovered with high support (1.0 pp and 99 bs), sister to the clade *P.* cf. *crassipes* – *P.* cf. *gracilis*. *Paraphronima* sp. A was also recovered with good support (1.0 pp and 88 bs), but recovered in an unresolved position. *Paraphronima* cf. *crassipes* (1.0 pp and 99 bs) formed a well-supported clade sister to *Paraphronima* sp. B, which in turn were sister to *P.* cf. *gracilis*. Specimens making up the *Paraphronima* sp. clade and a *P. gracilis* GenBank sequence (EF989674) were also recovered in an unresolved position.

### 3.2. Species delimitation

The four delimitation methods employed recovered one to ten species-level lineages (hereafter referred to simply as lineages) depending on either single or combined markers for the Yule Process and Coalescent tree priors (Table 2). The GMYC model was only statistically significant for the COI, COI+18S and COI+16S + 18S datasets (i.e. corresponding to a total of 9–10 consistently composed lineages; Table 2, Fig. 2D warm color bars), suggesting that the strongest signal is coming from the COI data. For the mPTP and bPTP analyses, estimates ranged respectively between 3–8 and 4.5–10 lineages, with the lowest number of lineages found for the combinations of 16S, COI+16S and 16S + 18S. The ABGD model for the single markers recovered six lineages for COI and four for 16S (Table 2, Fig. 2D).

When comparing the delimitation results to the clades in the concatenated gene tree, differences between the delimitation models were mainly caused by six sequences either splitting from or lumping with the main clades (Fig. 2D). These six outlier sequences included the GenBank sequence for *P. gracilis* from Monterey Bay (EF989674), the GenBank *Paraphronima* sp. sequence from the South China Sea (HM053501) and four sequences from Monterey Bay (*P. robisoni* sp. nov. USNM1429799, *Paraphronima* sp. B USNM1423164 and 1449303 and *P.* cf. *gracilis* USNM1423172). The GMYC and bPTP (i.e. ultrametric tree) models agreed in recognizing these latter six sequences as distinct entities. The mPTP model was slightly more conservative, finding only a single lineage within the *P. robisoni* sp. nov. and *Paraphronima* sp. A clades (Fig. 2D). The ABGD model predicted the lowest number of species-level lineages, six for COI and four in 16S. The main differences between the ABGD results were that 16S found no distinction between *P.* cf. *crassipes* and *Paraphronima* sp. B, and in COI, analyses recovered the published *Paraphronima* sp. (EF98674) as a separate lineage. Most of the polytomous *Paraphronima* sp. specimens (with exception of USNM1423172) were recognized as belonging to the *P.* cf. *gracilis* clade in all species delimitation analyses.

The lineages for *P.* cf. *crassipes*, and *P.* cf. *gracilis* are further supported by geographic locality, as both were exclusively and respectively collected from off Cabo Verde and Monterey Bay (Fig. 2D). Although the separation of *Paraphronima* sp. B from *P.* cf. *crassipes* was only supported in delimitation models that included COI, these specimens can be differentiated based on locality, as *Paraphronima* sp. B specimens were only collected from Monterey Bay. The lineages for *P. robisoni* sp. nov. and *Paraphronima* sp. A showed up in multiple locations (Fig. 2D). For *Paraphronima* sp. A, however, this was due to the outlier GenBank sequence from the South China Sea (HM053501) with the remainder collected off Cabo Verde. The lineage for *P. robisoni* sp. nov. had no single geographic locality with specimens from the Gulf of California, Monterey Bay and Cabo Verde.

The Yule Process and Coalescent tree priors had little effect on the suggested species-level lineages, although confidence intervals and likelihood ratios differed slightly across the priors. Implementation of the non-ultrametric ML tree in the PTP methods induced more variability into their estimates, causing the mPTP model to be more conservative than its ultrametric counterpart, while leading the bPTP model to infer one of the highest numbers of lineages out of all the methods (e.g. 15 for the COI+16S combination).

The genetic distances among and between the clades further reflect the observed signal for each of the genetic markers. The genetic distances for the COI marker ranged between 0 and 3.4% base substitutions within clades, and 10.5–28.6% between clades. For 16S, distances were much lower, measuring 0–0.7% within and 0.7–14.6% between clades. The number of base substitutions for the 18S marker was only minimal, with most divergent sequences differing only by 1.7%. As a result, the 18S marker was not variable enough to be informative for these species delimitation analyses.

**Table 2**
Species delimitation results for various datasets and models of *Paraphronima* using GMYC, mPTP, bPTP and ABGD methods on COI, 16S rRNA and 18S rRNA.

| | GMYC | Likelihood ratio | P | mPTP | bPTP | ABGD |
|---|---|---|---|---|---|---|
| | ML ent. (C.I.) | | | Est. ent. | Mean est. ent. (C.I) | Est. ent. |
| Coalescent | | | | | | |
| COI | 9 (8–10) | 14.13 | 0.0009* | 7 | 8.84 (7–12) | 6 |
| 16S | 2 (1–8) | 2.79 | 0.2479 | 3 | 4.54 (3–7) | 4 |
| COI+16S | 4 (1–11) | 3.03 | 0.2201 | 3 | 4.68 (3–10) | na |
| COI+18S | 9 (8–10) | 11.73 | 0.0028* | 7 | 8.99 (8–12) | na |
| 16S + 18S | 4 (1–11) | 3.03 | 0.2201 | 3 | 4.68 (3–10) | na |
| COI+16S + 18S | 10 (9–12) | 11.03 | 0.0040* | 8 | 10.17 (9–13) | na |
| Yule | | | | | | |
| CO1 | 9 (8–10) | 14.62 | 0.0007* | 7 | 8.94 (8–12) | |
| 16S | 2 (1–8) | 2.77 | 0.2502 | 3 | 4.58 (3–7) | |
| COI+16S | 4 (1–11) | 2.95 | 0.2293 | 3 | 4.71 (3–9) | |
| COI+18S | 9 (8–10) | 11.99 | 0.0023* | 7 | 9.01 (7–13) | |
| 16S + 18S | 4 (1–11) | 2.95 | 0.2293 | 3 | 4.71 (3–9) | |
| COI+16S + 18S | 10 (9–12) | 10.95 | 0.0042* | 8 | 10.27 (9–14) | |
| RaxML | | | | | | |
| COI | | | | 6 | 9.55 (7–16) | |
| 16S | | | | 1 | 5.09 (1–9) | |
| COI+16S | | | | 5 | 15.08 (12–21) | |
| COI+18S | | | | 6 | 7.75 (6–13) | |
| 16S + 18S | | | | 1 | 6.78 (1–12) | |
| COI+16S + 18S | | | | 8 | 9.57 (7–17) | |

*$p < 0.05$.

### 3.3. Systematics

Class MALACOSTRACA.
Order AMPHIPODA.
Suborder HYPERIIDEA.
Family PARAPHRONIMIDAE Bovallius, 1887.
Genus *Paraphronima* Claus, 1879.
*Paraphronima robisoni* sp. nov.
(Fig. 3, 4 and 5C, 6 and 7C).
LSID: urn:lsid:zoobank.org:pub:6C4D1D09-3CA9-4792-9128-85E2451F343B.

### 3.4. Type material

Nine females, four males and one juvenile specimen were collected in the Farallon (25.4417°N 109.848°W), Cerralvo (24.278°N 109.360°W) and Pescadero (24.310°N 10.213°W) basins, southern Gulf of California, México, from 20 to 1600 m depth between February 22 and March 1, 2015. One ovigerous female was chosen as the holotype and deposited at the Smithsonian National Museum of Natural History (USNM), Washington, D.C., as USNM1291026. Remaining specimens were deposited as paratypes (Table 1). Specimens used for genetics were either placed whole, when they were extremely small or damaged, into extraction buffer or pleopods were removed to extraction buffer and the remainder of the animal was fixed in 95% ethanol or 4% formalin.

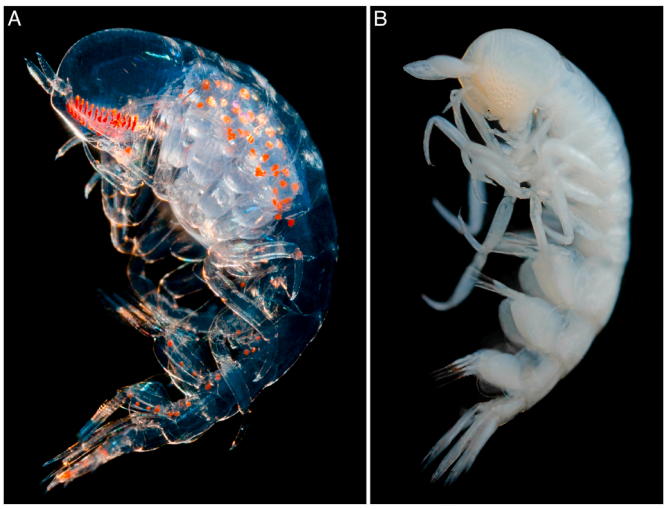


**Fig. 3.** *Paraphronima robisoni* sp. nov. types. (A) Live female holotype, USNM1291026 and (B) ethanol (95%) fixed male paratype, USNM1615585.

### 3.5. Other material examined

All *P. crassipes* and select *P. gracilis* specimens in the USNM collection were examined and reidentified, revealing *P. robisoni* sp. nov.-like morphotypes near the Straits of Florida (USNM1269491), Hawaii (USNM1242926), Panama (USNM1242914) and between Japan and the Philippines (USNM1242925). The samples from Japan and the Philippines were >10 mm, larger than the specimens from all the other localities. In addition to the morphotypes from other localities, genetic analyses revealed a *P. robisoni* sp. nov. specimen from Monterey Bay (USNM1429799) and another from off Cabo Verde Islands (USNM1450913), however, since these entire specimens were very small and used completely for DNA extraction, we could not confirm their morphology.

### 3.6. Etymology

The new species *Paraphronima robisoni* sp. nov. is named after Bruce H. Robison in recognition of his pioneering exploration of the midwater and numerous contributions to our understanding of midwater animals and their ecology. Also, for his mentoring of VIS, HJH, and KJO. The taxonomic description and underlying molecular justification for *P. robisoni* sp. nov. was prepared by VIS and KJO, who are responsible for making the specific name *robisoni* available.

### 3.7. Type locality

Gulf of California, México.

### 3.8. Diagnosis

Body length (from front of head to distal tips of uropods) up to 11.4 mm. Head slightly more in height than length, approximately same length as first three pereonites (PI–III; Fig. 4). Pereonites I and II (PI–II) together smaller in dorsal length than PIII (Fig. 4). Gills on coxae pereonite V, approximately same length as basis of fifth pereopod (P5; Fig. 4). Posterior margin of pereopods 3–4 and anterior margin of pereopods 5–7 bear few small or no setae on ischium to propodus, visible only with high magnification (Fig. 4 and 7C). Pereopods 7 similar in length to P6 or only slightly shorter (Fig. 4). Epimeral plate of pleonite I with ventral margin nearly perpendicular to antero-posterior body axis, nearly as broad ventrally as dorsolaterally (Fig. 4 and 7C).

### 3.9. Description holotype (Fig. 3 and 4)

Total length female holotype 9.7 mm, body transparent with several red-pigmented, vertically-oriented chromatophores. Chromatophores located superficially on lateral sides of pereon with fewer on lateral sides pleon, pleopods, buccal mass, and dorsal side third uropod pair. Head cuboid, height slightly greater than length (i.e. measuring the longest dorsoventral and anteroposterior axes, respectively), approximately equal length to first three pereonites. Ventrally projecting cephalon, extending half its height below the attachment to the body at the ventral midline. Antennae 1 inserted anteriorly on cephalon, with a three-articulate base and flagellum. Antennae 1 approximately half length of head, peduncle slightly more in width than flagellum; medial surface flagella bear setae along length-axis, smaller setae clustered at apex. Antennae 2 inserted ventrally on cephalon, anterior to buccal mass; two articles, similar in length to antennae 1.

Pereonites unfused. Pereonites I and II similar in dorsal length, together approximately equal length to pereonite III. Pereonites IV–VII similar in dorsal length, PVI–VII slightly shorter in height (ventral-dorsal) than preceding ones. Pereonites III–VI with gills, various lengths. First gill pair approximately $^{1}/_{3}$ length of corresponding basis, followed by ½, 1 and ¾ basis length for the second, third and fourth pair, respectively. Coxal plates PII-V free.

Gnathopod 1, basis width slightly more than $^{1}/_{3}$ length, slightly longer than combined length of ischium through dactyl. Gnathopod 1 merus forms a small cup with several spines posterodistally; carpus flattened posterodistally, few spines at apex; propodus slightly shorter than carpus, forming weak subchela when bent; dactyl small, cone shaped. Gnathopod 2 basis width ¼ of its length and approximately equal in length to combined length ischium through dactyl. Gnathopod 2 carpus longer than propodus and dactyl combined, dactyl with triangular lobe at base; length G2 longer than G1. Pereopods 3–6 similar, approximately twice as long as G2, basis width slightly more than $^{1}/_{3}$ of length and somewhat shorter than combined length ischium through dactyl. Pereopods 3–4 facing backward, P5–7 facing forward. Pereopods 3–7 bear small, delicate, evenly spaced setae on either posterior (P3–4) or anterior (P5–7) margin of ischium through propodus; carpus five times longer than wide, propodus narrower and slightly shorter than carpus, dactyl small. Pereopod 7 similar to preceding pairs and approximately same length, but basis slightly longer with a concave anterior and convex posterior margin.

Pleon approximately half length pereon. Pleonites similar in width to each other, pleonite III ¾ height of pleonite I–II. Epimeral plates of pleonites evenly rounded, ventral margin nearly perpendicular to antero-posterior body axis, approximately equal width at base of lobe and distal portion. Pleopod basis almost same length as corresponding epimeral plates, decreasing slightly in size from first to third pair. The pleopod basis shows moderate levels of sexual dimorphism in all *Paraphronima* species with female basises elongated, length approximately twice width.

Urosome with urosomites equal in length. Uropod basipodites approximately equal in length, width increasing from first to third pair. Uropod 1 endopodite elongated, triangular, with serrations on both sides, half the length of its basis, exopodite $^{2}/_{3}$ width of endopodite, serrations on medial side only. Uropod 2 endopodite elongated, triangular, narrower than endopodite U1, with serrations on both sides, $^{2}/_{3}$ the length of basis, exopodite lanceolate, only half the width of endopodite and slightly shorter. Uropod 3 endopodite triangular, with serrations on both sides, approximately $^{1}/_{5}$ length of basis and nearly half length of endopodites U1 and 2, exopodite half width endopodite with serrations on medial side.

### 3.10. Sexual dimorphism

Males similar in body morphology to females except for following. Total body length up to 8.3 mm. Presence of chromatophores not

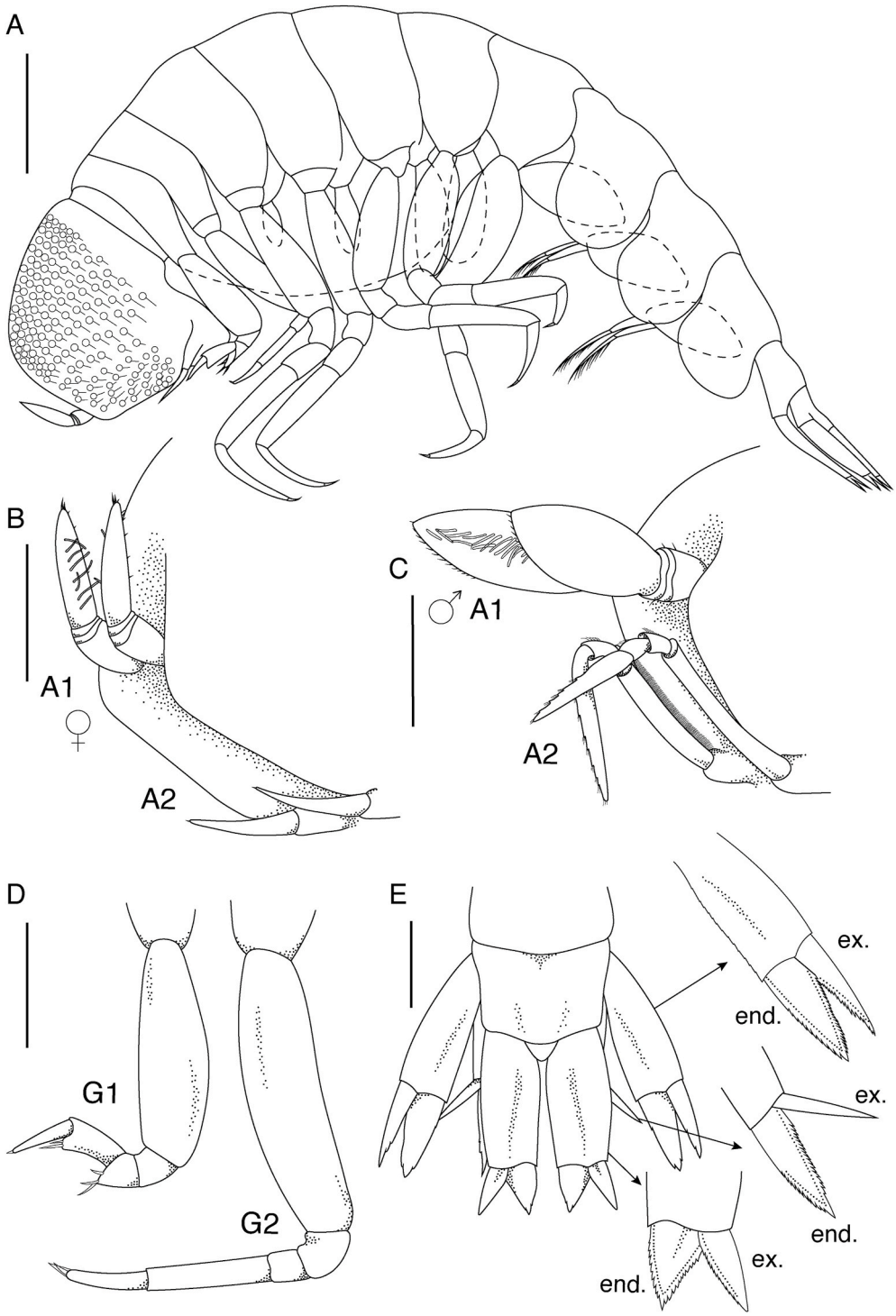


**Fig. 4.** *Paraphronima robisoni* sp. nov. (A) Female holotype, 9.7 mm, from Gulf of California, México. (B) First (A1) and second (A2) antennae pair, female. (C) First and second antennae pair, male. (D) Gnathopods 1 (G1) and 2 (G2) and (E) Urosome with details of exopodite (ex.) and endopodite (end.) uropods. Scale bar is 1 mm in A, 0.25 in B, C, and 0.5 in D, E.

confirmed. Antennae 1 slightly shorter than head length (Fig. 3B and 5C), with elongate and broad flagellum (Fig. 4C). Antennae 1 flagellum wider than peduncle, multiple rows (>10) of aesthetascs on medial surface flagellum, running perpendicular to long axis; peduncle with few, thin setae. Antennae 2 about 1¼ length of antennae 1, consisting of four articles with first and fourth article elongate, small setae on fourth segment (Fig. 4C). Coxal plates of pereonites fused. Pleopod basis rounded, length approximately same size as width.

### 3.11. Distribution

*Paraphronima robisoni* sp. nov. was primarily found in the Gulf of California, México (Eastern Tropical Pacific), just outside the Monterey Bay (Eastern North Pacific), as well as near the Cabo Verde Islands (Eastern North Atlantic Ocean). *Paraphronima robisoni* sp. nov. occurs from the surface down to at least 800 m depth (Table S1). It may occur deeper as one specimen was caught by a net towed from 3000 m to the surface.

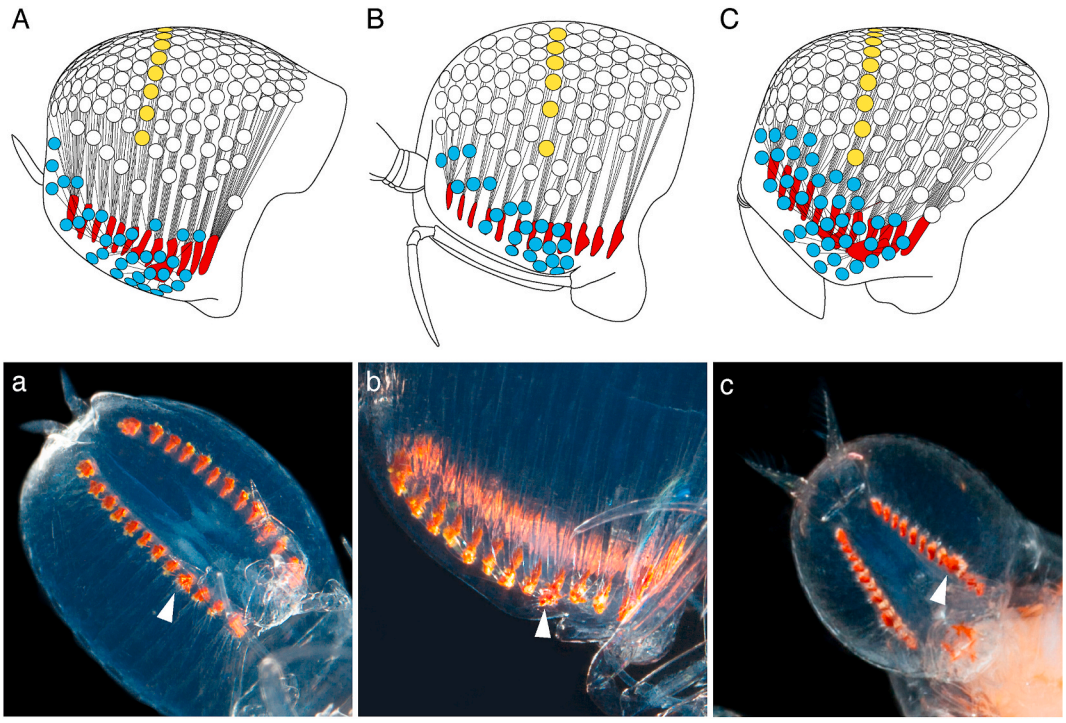


**Fig. 5.** Eyes of (A, a) *Paraphronima* cf. *gracilis,* (B-b) *Paraphronima* cf. *crassipes* and (C-c) *Paraphronima robisoni* sp. nov. (A–C) Illustration of left eyes for each of the three species listed, showing the organization of upward-facing ommatidia (white circles, a single dorsally-directed row in yellow) and lateral-facing ommatidia (blue circles). (a–c) Close-up views of the twelve discontinuous retinas per eye and the primary lateral retina (white arrow), which can be seen on the side of the ninth retina. (a) *Paraphronima* cf. *gracilis* as seen from below, (b) *P.* cf. *crassipes* in profile and (c) *P. robisoni* sp. nov. as seen from below. (For interpretation of the references to colour in this figure legend, the reader is referred to the Web version of this article.)

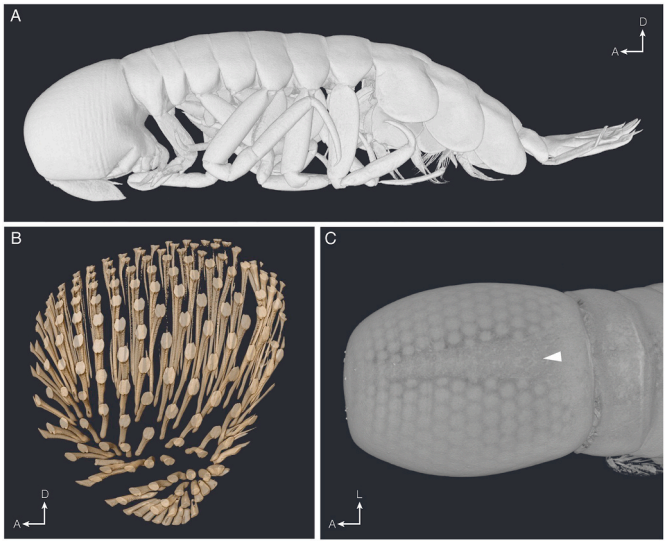


**Fig. 6.** 3D reconstruction of the male paratype *Paraphronima robisoni* sp. nov. (USNM1615585) with micro-computed tomography (microCT). (A) Overview full body. The fifth ischium to dactylus was broken off and is therefore not visible in this image. (B) Isolated view crystalline cones in left eye (i.e. part of ommatidial facets). (C) Exterior view head with ommatidial break visible at dorsum, 2–3 ommatidia wide indicated by white arrow (visible as grey streak between ommatidial lenses).

### *3.12. Eye morphology*

The most obvious difference between *P. robisoni* sp. nov. and known *Paraphronima* species is the structure of their eyes (Fig. 5). In all *Paraphronima*, the 16 to 18 mostly dorso-laterally oriented rows of ommatidia have their darkly pigmented rhabdoms closely packed into 12 clusters, or discontinuous retinas, that are easily visible within the transparent body. The retinas form a row for each eye aligned along the long axis of the ventral portion of the head (Fig. 5). The anterior- and posterior-most retinas consist of three or four tightly spaced rows, while the ten retinas between these terminal retinas each support a single row of ommatidia (with the exception of retina nine, see below). This variability in number of rows makes it difficult to consistently name the rows and assign them to a retinal group. Moreover, the variability in the number of ommatidial rows may be gender specific, with males having 16 or 17 rows of ommatidia while females typically have 18 rows. All ommatidial rows contain 2–10 units that fan out in a plane perpendicular to the body axis, as well as 0–7 (but see retina nine below) ommatidia of each row that differ from this dorso-ventral fan pattern, instead being directed anteriorly, ventrally or posteriorly, depending on where they are in the eye. These ommatidia stem from the lateral ends of each dorsal ommatidial row, and patterns in their number and direction differ between species (Fig. 5A–C). Individual non-dorsally directed ommatidia stemming from retinas anterior to retina 9 (retinas 1–8 or ommatidial rows 1–10 or 11) are directed anteriorly and laterally, while non-dorsally directed ommatidia posterior to retina 9 (retinas 10–12 or ommatidial rows 12 or 13–16, 17 or 18) are directed posteriorly. In contrast to all the other retinas, the lateral portion of the ninth retina, or the primary lateral retina, has a near-radial arrangement of up to 28 ommatidia, which form the majority of the non-dorsally directed ommatidia, and together, are referred to as the “lateral eye” (Fig. 5a–c). The crystalline cones of these non-dorsally directed ommatidia tend to be substantially shorter than those of the dorsally-directed ommatidia (Fig. 6B).

The differences between species observed in the eyes are most clear in the relative size of their heads (Fig. 7) and the arrangement of the lateral portions of the eyes (Fig. 5A–C). In *P. robisoni* sp. nov., it is difficult to tell the dorsally directed ommatidia from the anteriorly or

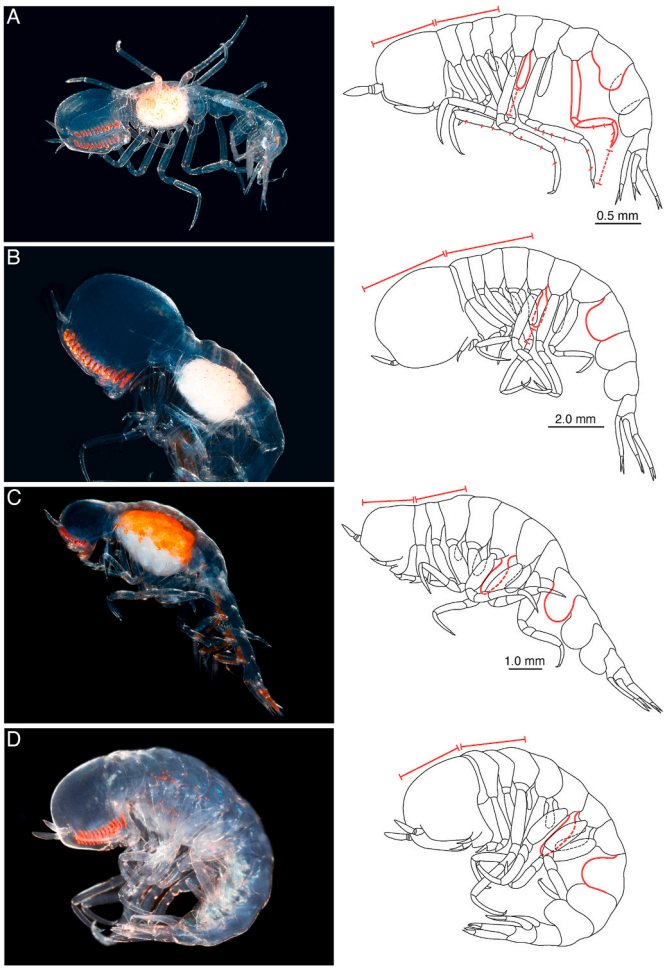


**Fig. 7.** Live specimens of *Paraphronima* and illustrations of each species with their key identifying characteristics. (A) *Paraphronima gracilis*, (B) *Paraphronima crassipes*, (C) *Paraphronima robisoni* sp. nov. and (D) *Paraphronima* sp. A. Red lines in illustrations on the right indicate differences in head size (measured relative to the pereonites), length of peronite V gill pair (measured relative to the P5 basis), shape of pleonite I epimeral plate, length of pereopod 7 (relative to P6) and presence of setae visible without magnification. A and B adapted from Zeidler (2003). Scale bar for D not available, relative body size not to scale. (For interpretation of the references to colour in this figure legend, the reader is referred to the Web version of this article.)

laterally directed ones because they form an evenly spaced pattern of facets. In contrast, in *P.* cf. *crassipes* and *P.* cf. *gracilis*, there is a clear break in the facet pattern between laterally and dorsally directed ommatidia, with the dorsally directed ones forming a roughly v-shaped margin that points towards the "lateral eye" (Fig. 5A and B). Additionally, in *P. robisoni* sp. nov., the anteriorly directed ommatidia in rows 2–6 of the lateral eye are more numerous and change angle from the dorsal fan nearly 90°, instead of less than 45°. A further difference between the species is that *P. robisoni* sp. nov. contains more than twice as many ommatidia in the primary lateral retina than *P.* cf. *crassipes* or *Paraphronima* sp. A. ($28 \pm 1$ SD $n_{eyes} = 2$; $12 \pm 1$ SD $n_{eyes} = 2$; $11 \pm 1$ SD $n_{eyes} = 8$, respectively). Similarly, the number of additional ommatidia that were not directed dorsally, nor part of the primary lateral retina, were greater in *P. robisoni* sp. nov. ($30 \pm 5$ SD, $n_{eyes} = 2$) than in *P.* cf. *crassipes, P.* cf. *gracilis* and *Paraphronima* sp. A ($20 \pm 1$ SD $n_{eyes} = 2$; $26 \pm 3$ SD $n_{eyes} = 4$; $16 \pm 11$ SD $n_{eyes} = 8$, respectively). Finally, in *P. robisoni* sp. nov., the two eyes are dorsally separated by a gap equivalent to at least the width of two ommatidia (Fig. 6C), while this gap measures less than a single ommatidium in *P.* cf. *gracilis*, *P.* cf. *crassipes* and *Paraphronima* sp. A.

Detailed examination of the eye structure of *Paraphronima* sp. A, beyond the few microCT scanned specimens reported above, was not possible due to COVID19 closure of the USNM collections and laboratories. These species will be the subject of a later publication when access to specimens is possible.

### 3.13. Remarks

Morphologically, *P. robisoni* sp. nov. was most similar to *P. crassipes*, and examination of *Paraphronima* in the USNM collection revealed multiple specimens previously identified as *P. crassipes* that are actually *P. robisoni* sp. nov. or one of the other probable new species. *Paraphronima robisoni* sp. nov. differs from *P. crassipes* and *P. gracilis* in its small body size, relatively small head, length of the gill pair on the fifth pereonite, distance between the eyes on the dorsal surface of the head, number of facets in the primary lateral retina, and minimal distinction between the dorsally and laterally directed ommatidia (Table 3, Fig. 7, see Supplementary Results for key to species). *Paraphronima gracilis* and *P. crassipes* are generally larger in body length (up to 17 and 31 mm respectively; Zeidler, 2003), with the gill pair on PV approximately $^{2}/_{3}$ length of the corresponding PV basis (Fig. 7A and B). Additionally, they have heads greater in length than the first three pereonites, a gap between the eyes at the dorsum that is smaller than the size of one ommatidium, and a clear break between the dorsally and laterally directed ommatidia (Fig. 5 and 7). In *P. gracilis,* pereonite I and PII are

**Table 3**
Comparison of key characteristics to distinguish *Paraphronima* species.

| Character | *Paraphronima gracilis* | *Paraphronima crassipes* | *Paraphronima robisoni* sp. nov. |
|---|---|---|---|
| Body length (dorsal midline, including urosomite) | Up to 17 mm, usually 10 mm | Up to 31 mm, usually 20–24 mm | Up to 11.4 mm. |
| Head length (Antero-posterior axis) | Head > PI–III | Head ≥ PI–IV combined | Head ≃ PI–III combined |
| Pereonite length (dorsal midline) | PI–II < PIII | PI–II < PIII or PI–IV each equal | PI–II combined ≥ PIII |
| PV gill length | ~ $^{2}/_{3}$ P5 basis | ~ $^{2}/_{3}$ P5 basis | ≃ P5 basis |
| Basipodites pereopods | Slender | Broad | Broad |
| Setae pereopods 5–7 (anterior margin ischium to propodus) | Small robust setae (visible with low magnification light microscope) | Few or no robust setae | Few or no robust setae |
| Pereopods 7 length | Not > P6 basis–carpus | Same length or only slightly shorter than P6 | Same length or only slightly shorter than P6 |
| Pleonite 1 epimeral lobe | Approx. half-length PLI at dorsal midline (anterior margin forms ~45° angle to body axis) | Equal length PLI at dorsal midline (anterior margin perpendicular to body axis) | Equal length PLI at dorsal midline (anterior margin perpendicular to body axis) |
| Dorsal and ventro-lateral facets separated by a clear break | Yes | Yes | No |
| # ommatidia primary lateral retina | ~20 | ~12 | ~28 |
| Eyes dorsally separated by space X facets wide | <1 | <1 | 2–3 |

smaller in dorsal length than PIII, while in *P. crassipes,* PI–IV are equal in length according to Vinogradov et al. (1996) and Zeidler (2003). However, we observed some variability in this characteristic, with PI and PII sometimes smaller in dorsal length than PIII in *P. crassipes*. Similar to *P. robisoni* sp. nov., the pereopod basises of *P. crassipes* are broad, the setae on P3–7 are small or absent, P7 is similar or slightly shorter in length to P6, and the epimeral plates of PL1 is evenly rounded (Fig. 7B). In contrast to *P. robisoni* sp. nov., the pereopod basises in *P. gracilis* are slender, the setae of P3–7 robust, the length of P7 does not exceed the carpus of P6, and the epimeral plates of PLI are approximately half the length of the PL1 dorsal midline (Fig. 7A).

Five of the six unaccepted *Paraphronima* species matched the descriptions of either *P. crassipes* or *P. gracilis*, while *Hyperia pedestris* Guérin-Méneville, 1836 (unaccepted) was similar to *P. robisoni* sp. nov. based on the type locality and its relatively small body size (7 mm). *Hyperia pedestris* (unaccepted) was described in 1836 by Guérin-Méneville off the coast of Chile and was recognized as *Paraphronima pedestris* (unaccepted) by Bovallius in 1889. When Zeidler rediscovered the holotype in 1995 (Academy of Natural Sciences, Philadelphia, CA2698 Guérin-Méneville Coll., no 432), the author found the specimen desiccated with no appendages intact (Zeidler, 1995). Despite the partly destroyed remains, Zeidler (1995) was able to determine the shape of the epimeral plate on pleonite I as matching that of *P. crassipes*. Given the destroyed holotype and that Guérin-Méneville (1836) did not include a detailed description of the species, we unfortunately only have the drawing of *H. pedestris* provided by Guérin-Méneville for comparison to our specimens. We conclude that *H. pedestris* is not *P. robisoni* sp. nov. due to the following four differences: *H. pedestris*' head is approximately equal in length to the first two pereonites combined, a feature more similar to *Hyperia*; gills on the fifth pereonite measure $^{2}/_{3}$ of the corresponding basis length, more characteristic of *P. crassipes*; pereopod seven is much smaller than P6, generally seen in *P. gracilis*; and the pereopods appear more slender and elongate than in *P. robisoni* sp. nov. Based on these differences, *H. pedestris* does not conform to the description for *P. robisoni* sp. nov. nor that of *P. crassipes*.

The accuracy of the Guérin-Méneville (1836) illustration is questionable given the stylization and lack of realistic detail. More importantly, the way the gills on pereonite V-VII are drawn is clearly incorrect because gills do not occur on PV–VII of most hyperiids, but instead on PIII-VI. Given that we will never be able to determine the morphological details of *H. pedestris* because of the destroyed holotype, inadequate illustration and description, and because the binomen *H. pedestris* was suppressed by the International Commission on Zoological Nomenclature (ICZN, 1997) in favor of *P. crassipes*, we conclude that it is most appropriate to leave *H. pedestris* suppressed. We therefore create the new name, *P. robisoni*, for the species described here from the Gulf of California.

Although we could not physically investigate *Paraphronima* sp. A and sp. B due to COVID19 pandemic restrictions, there is evidence to further differentiate *Paraphronima* sp. A from *P. robisoni* sp. nov. Photographs of two freshly caught individuals of *Paraphronima* sp. A showed that most of their body and appendage morphology is similar to *P. robisoni* sp. nov. (Fig. 7D), but with a few notable differences. *Paraphronima* sp. A appeared larger in total body length and their head measured approximately the same length as the first 3.5 pereonites combined. Furthermore, the eye morphology of *Paraphronima* sp. A was distinctly different from *P. robisoni* sp. nov., being more similar to *P. crassipes*.

## 4. Discussion

### 4.1. Paraphronima eyes

All *Paraphronima* eyes have (*i*) twelve discontinuous retinas, (*ii*) both dorsally and ventro-laterally directed ommatidia, (*iii*) a roughly similar number of dorsally directed ommatidia and (*iv*) a primary ventro-lateral group of ommatidia connected to the ninth retina from the anterior. Differences between the species were most obvious in the ventro-lateral portions of the eyes. *Paraphronima robisoni* sp. nov. had the least distinction between dorsally and laterally directed facets with many more ommatidia deviating from the primarily dorsally directed orientation. Although *P. robisoni* sp. nov. and *Paraphronima* sp. A were genetically most closely related and shared many morphological similarities, the arrangement of their ventro-lateral ommatidia were the most distinct from each other. The eyes in *Paraphronima* sp. A, *P.* cf. *crassipes* and *P.* cf. *gracilis*, on the other hand, were surprisingly similar, despite their genetic dissimilarity and distinct body and appendage morphology. Consequently, when the arrangement of the eyes can be made visible through preservation or staining, they can serve as additional characters to distinguish *Paraphronima* species. Body morphology, for instance, provides clear distinction between *P. gracilis* and *P. crassipes*, while eye morphology clearly differentiates *Paraphronima* sp. A and *P. crassipes* from *P. robisoni* sp. nov. It remains to be seen if morphology also supports the genetic differences found between *Paraphronima* sp. A and *P. crassipes*.

In addition to these species-specific differences found in the eye morphology, our results suggest possible differentiation in the eyes between the sexes. Although Land (1989) noted that hyperiids usually lack sexual dimorphism in the structure of their eyes, the male *Paraphronima* specimens consistently had fewer rows of dorsal ommatidia (i.e. 16–17, as opposed to 18 in females). Further research is needed to determine whether males have fewer ommatidia because of their relatively smaller body size or if they use this extra space to increase facet diameter - and thereby light sensitivity - to potentially better detect the low contrast silhouettes of females. Visual adaptations to improve the detection of females are a well-known feature of male insects such as dipteran flies, where males tend to have larger facets and higher visual acuity to track their female counterparts against the backdrop of the sky (Zeil, 1983; Land, 1989; Meyer-Rochow, 2015). Similar to male insects, hyperiid males are thought to pursue conspecific females (Harbison et al., 1977), evidenced by adaptations such as enlarged sensory antennae (Vinogradov et al., 1996) and greater swimming speeds when compared to females (Harbison et al., 1977). Nevertheless, since recognition of conspecifics in amphipods is thought to be based on chemosensory signals (Hallberg and Skog, 2011), additional microCT scans and detailed analysis of their eye structure is needed to document gender and phenotypic differences within and between species.

The differences in eye morphology between hyperiidean genera is often dramatic and is seldom illustrated or described in any detail. However, these gross differences can be incredibly useful in identification of certain genera. Differences in eye morphology are most obvious in live specimens but typically easily visible in fixed specimens. In spite of compound eyes becoming less transparent through preservation (e.g. Fig. 3A vs. 3B), the crystalline cones can be easily distinguished from their interstitial surroundings through the differential diffraction of light. As such, when illuminated by light, the orientation and number of crystalline cones can be quantified. We suggest that eye characters should be completely described, illustrated and included in all future descriptions. Further, our findings here suggest that eye morphology may provide valuable characters for distinguishing cryptic diversity within the Hyperiidea. For example, we have seen that *P. robisoni* sp. nov. was frequently identified as *P. crassipes* in the USNM historical collection, a mistake easily made if ignoring the eyes. Similarly, *Lanceola sayana* Bovallius, 1885 and *Scypholanceola aestiva* (Stebbing, 1888) both key to *L. sayana*, with the only difference being their dramatically different eyes. We therefore recommend inclusion of eye morphology in future taxonomic studies of Hyperiidea given the few characters available for these animals and our finding that eye characters can be useful to distinguish even species level taxa.

### 4.2. Paraphronima species diversity

Based on our phylogenetic analyses, at least five clades of genetically

distinct species-level clades could be identified within *Paraphronima*, including *P. robisoni* sp. nov., *Paraphronima* sp. A, *P.* cf. *crassipes*, *Paraphronima* sp. B and *P.* cf. *gracilis* (Fig. 2D). These clades are further supported by morphological characters (see above Remarks) or by geographic locality in the case of *Paraphronima* sp. B. Our results strongly suggest hidden genetic complexity within the genus given that our species delimitation models generally inferred an even higher number of species level clades than the five identified here (i.e. up to 15, Fig. 2D, Table 2). However, these additional putative species require further investigation and additional sampling because they are mainly singletons, unsupported clades or odd sequences.

Even though we only describe a single new species here, we have genetic support for a second species, referred to as *Paraphronima* sp. A. Once we are able to access the complete USNM collections again, we will examine the specimens genetically identified as *Paraphronima* sp. A for morphological characters that distinguish them from other *Paraphronima* species. Considering that *P. robisoni* sp. nov. and *Paraphronima* sp. A were genetically distinct but collected in the same trawl nets from the eastern tropical Atlantic Ocean, suggests they are genetically isolated in sympatry. Intriguingly, *Paraphronima* sp. A showed strong similarity to historical USNM specimens collected from the Philippines and Japan (USNM1242925), which were also larger in body size. Unfortunately, it is not possible to obtain genetic sequences from these historical specimens. Based on geographic proximity, it could be argued that the specimens from Japan and Philippines are related to the unidentified *Paraphronima* sp. sequence from the South China Sea (GenBank, HM053501), which grouped with specimens of *Paraphronima* sp. A (Fig. 2). Consequently, we suspect that detailed investigation of *Paraphronima* sp. A and those from Japan and the Philippines may reveal a fourth morphologically distinct species.

While *P. robisoni* sp. nov., *P.* cf. *crassipes* and *Paraphronima* sp. A are clearly distinct species in all phylogenetic and species delimitation analyses, putative species *Paraphronima* sp. B is less well-supported. Thus, *Paraphronima* sp. B requires further sampling and examination of specimen morphology to determine its status. One of the *Paraphronima* sp. B specimens, for instance, was previously identified as *P. crassipes* (USNM1284376), yet was genetically distinct from the *P.* cf. *crassipes* clade (>10% base substitutions, Fig. 2D). Phylogenetic analyses of COI and all species delimitation analyses that included COI data returned *Paraphronima* sp. B as a species-level clade distinct from *P.* cf. *crassipes*. Since all *Paraphronima* sp. B were collected in the northeastern Pacific, but all *P.* cf. *crassipes* in the North Atlantic, it is plausible that both are genetically isolated. Further sampling is required to determine whether our *P.* cf. *crassipes* specimens represent *P. crassipes* Claus (1879), as the holotype locality for the latter is in the Mediterranean Sea.

*Paraphronima gracilis* is a difficult species to define in our analyses given that we recovered a well-supported clade, as well as a number of sequenced individuals with consistent genetic variation fitting the morphological description of *P. gracilis*. Species delimitation analyses consistently grouped these together but phylogenetic clades composition was not consistent between genes, nor were those clades well supported (Fig. 2). In addition, all specimens identified in this study as belonging to *P. gracilis* were collected in the northeastern Pacific while the type locality of *P. gracilis* is the Atlantic Ocean. Although it is not unheard of for an open ocean species to have a distribution range that legitimately covers multiple ocean basins, it will be necessary to collect specimens from the Atlantic to fully represent the genetic and morphological diversity of this species or what may be multiple species.

Even though we used a conservative integrative approach to investigate phylogenetic relationships within the genus *Paraphronima* (i.e. combining both molecular and morphological data), we found that further research into the evolutionary relationships within the genus are needed given the polytomies found for several *Paraphronima* samples (i.e. recognized as *Paraphronima* sp. in the concatenated gene tree). Although this polytomy is likely to be caused by the absence of the COI marker for nine out of the ten sequences, we suggest increased sampling and use of additional rapidly evolving markers to determine whether the polytomy represents an actual split between lineages. The 16S rRNA and the hypervariable region of the 18S rRNA marker proved too slow to be of particular use in this study.

In all, our data strongly suggests a higher level of diversity than expected within *Paraphronima*. Hidden diversity appears to be a common concept in the open ocean (Norris, 2000), with speciation in aquatic environments thought to be more closely linked to non-visible traits, such as chemosensory systems, rather than morphological divergence (Knowlton, 1993; Palumbi, 1994; Baird et al., 2011). Alternatively, limited sampling may not accurately represent the variability within a species and strong selective pressure may constrain visible morphological change within this vast habitat. Speciation can be driven on more local scales by both abiotic and biotic factors (Knowlton, 1993; France and Kocher, 1996; Norris, 2000). Not only is the water column structured by temperature, salinity, dissolved oxygen and nutrient availability, all of which can facilitate niche differentiation, additional features that may shape diversity include seasonality of current velocities, attenuation of downwelling solar illumination and the distribution of biological light (Knowlton, 1993; Norris, 2000; Widder, 2002). For example, abiotic factors related to depth were shown to drive niche differentiation in the bathyal amphipod *Eurythenes gryllus* (Lichtenstein in Mandt, 1822) where instead of one species distributed broadly over a wide depth range, there are actually multiple species found at different depth intervals (France and Kocher, 1996).

Although *Paraphronima* have been caught globally in temperate and tropical oceans (Zeidler, 2003; Burridge et al., 2017), their depth distribution has only been reported in a few studies. It is assumed that most individuals live in the upper 500 m of the water column since only a few specimens have been caught in nets deployed deeper than this (possibly as deep as 1100 m; Brusca, 1967; Thurston, 1976; Smith-Beasley, 1992; Vinogradov et al., 1996). In addition, some data suggests that *Paraphronima* undergoes shallow diel vertical migrations in the Northeast Pacific (Brusca, 1967; Smith-Beasley, 1992) and Northeast Atlantic (Thurston, 1976). More detailed documentation of *Paraphronima* and their depth distribution is needed to determine if and what physical factors might have driven their niche differentiation.

In addition, biological factors such as predator avoidance and prey or host selectivity can further promote species separation (Knowlton, 1993, 2000). Hyperiid amphipods are well known for their symbiotic associations with gelatinous zooplankton, with some hyperiids suggested to be generalists while others show a high degree of host-specificity (Harbison et al., 1977; Madin and Harbison, 1977; Laval, 1980; Harbison, 1998). Harbison (1998) noted that this host-specificity might be a way to minimize competition and thereby drive niche separation, exemplified by the hyperiids *Lycaea vincentii* Stebbing, 1888 and *Lycaea nasuta* Claus, 1879, that are exclusively and respectively found on the pelagic tunicates *Salpa cylindrica* Cuvier, 1804 and *Cyclosalpa affinis* (Chamisso, 1819) (Madin and Harbison, 1977). Harbison (1998) proposed that differential sensitivity to select allelochemicals (i.e. secondary metabolites released by the host to either deter or attract heterospecifics) may be the mechanism facilitating the host-hyperiid selectivity.

Although *Paraphronima* have been collected from gelatinous zooplankton, reports on their associations are rare (Lo Bianco, 1909; Harbison et al., 1977; Laval, 1980; Lavaniegos and Ohman, 1999; Gasca et al., 2015). When observed by remotely operated vehicles, *Paraphronima* are most often free-swimming (KJO personal observations). The few studies that report associations for *Paraphronima* suggest that they have a preference for small siphonophores, with specimens reported on *Rosacea cymbiformis* (Delle Chiaje, 1830) (Harbison et al., 1977; Laval, 1980; Gasca et al., 2015) *Diphyes* sp. Cuvier, 1817, *Sulculeolaria* sp. Blainville, 1830 (Lo Bianco, 1909) and *Sphaeronectes koellikeri* Huxley, 1859 (Lavaniegos and Ohman, 1999). One study also reported *Paraphronima* on the salp *Ritteriella picteti* (Apstein, 1904) (Lavaniegos and Ohman, 1999). As such, the degree of host-selectivity remains to be determined and further research might reveal

species-specific interactions once the 'cryptic' *Paraphronima* species are more accurately identified and more associations are recorded. The few associations reported for members of *Paraphronima* may also suggest that they are not tightly associated with any host, but instead primarily free-swimming hunters. It should, however, be noted that most hyperiids are thought to release their young on or within gelatinous zooplankton, as the otherwise small juveniles, that often lack adult characters and swimming strength, might fail to find food (Laval, 1980).

Finally, in addition to niche separation on local scales, genetic isolation by distance is another well-known driver of diversity in coastal, freshwater and deep-sea amphipods (Pilar Cabezas et al., 2013; Westram et al., 2013; Copilaş-Ciocianu et al., 2020). The main reason for this is the brooding mode of reproduction and extended parental care of most amphipods that limits their larval dispersal (Baird et al., 2011; Copilaş-Ciocianu et al., 2020). In Hyperiidea this pattern is unknown due to the scarcity of molecular data (Browne et al., 2007; Hurt et al., 2013), but has been shown in a few individuals of *Phronimella elongata* (Claus, 1862), *Phrosina semilunata* Risso, 1822 (Browne et al., 2007) and *Themisto libellula* (Lichtenstein in Mandt, 1822) (Tempestini et al., 2017). While *P. robisoni* sp. nov. and potentially *Paraphronima* sp. A appear to have broader geographic distributions, the other species-level clades were recovered from single localities. This suggests that species of *Paraphronima* are restricted smaller geographic scales than currently reported, although further sampling is warranted. In conclusion, there are a variety of physical and biological mechanisms that can cause species to become reproductively isolated in the open ocean. In the case of the three nominal *Paraphronima* species, where we know little of their biology, differences in their eye morphology suggests that their light environment or visual tasks may have played an important role in driving diversity.

## CRediT authorship contribution statement

**Vanessa I. Stenvers:** Formal analysis, Methodology, Investigation, Data curation, Writing – original draft, Visualization, Funding acquisition. **Brett C. Gonzalez:** Formal analysis, Methodology, Writing – review & editing. **Freya E. Goetz:** Formal analysis, Investigation, Data curation, Writing – review & editing. **Jan M. Hemmi:** Software, Formal analysis, Investigation, Resources, Writing – review & editing. **Anna-Lee Jessop:** Formal analysis, Investigation, Writing – review & editing. **Chan Lin:** Writing – review & editing. **Henk-Jan T. Hoving:** Resources, Writing – review & editing. **Karen J. Osborn:** Conceptualization, Methodology, Investigation, Resources, Data curation, Writing – review & editing, Visualization, Supervision, Project administration, Funding acquisition.

## Declaration of competing interest

The authors declare that they have no known competing financial interests or personal relationships that could have appeared to influence the work reported in this paper.

## Acknowledgements

We thank Bruce Robison for the invitation to participate in the expedition where the species was discovered, Herman Wirshing for his training of VIS in the Laboratory of Analytical Biology, Smithsonian National Museum of Natural History, Wolfgang Zeidler for his insights on the unaccepted *Paraphronima* descriptions, Rob Sherlock, Kim Reisenbichler, George Matsumoto, Susan Von Thun, Anela Choy and Unai Markaida Aburto for assistance at sea, and Rebeca Gasca for an early discussion of *Paraphronima* species off México. We thank the crew and pilots of the R/V *Western Flyer* and ROV *Doc Ricketts* for their support on multiple expeditions. The David and Lucile Packard Foundation provided funding to the Monterey Bay Aquarium Research Institute who supported these expeditions. We thank the crew of R/V *Poseidon* and the science team for support during POS520 and POS532, in particular Helena Hauss, Eduard Fabrizius, Hendrik Hampe and the JAGO team are thanked for help with collections of amphipods in Cabo Verde. Funding was provided for this fieldwork by the Smithsonian Institution Biodiversity Genomics/Global Genome Initiative Grants Program to KJO (SIBG/GGI 33GGI2014GRANTA), for the lab work by the Rathbun Endowment for Crustacean Research, and financial support for VIS to pursue this project at the Smithsonian Institution by the Holland Scholarship, Marco Polo Fund and the Groningen University Fund. Molecular benchwork was completed in and with the support of the Laboratories of Analytical Biology, Smithsonian Institution, National Museum of Natural History. HJH is funded by grant HO 5569/2–1 (Emmy Noether Junior Research Group) from the Deutsche Forschungsgemeinschaft (DFG). The eye analysis program was supported by the Australian Research Council Discovery Projects funding scheme (project number DP180100491).

## Appendix A. Supplementary data

Supplementary data to this article can be found online at https://doi.org/10.1016/j.dsr.2021.103610.

## References

Bagheri, Z.M., Jessop, A.-L., Kato, S., Partridge, J.C., Shaw, J., Ogawa, Y., Hemmi, J.M., 2020. A new method for mapping spatial resolution in compound eyes suggests two visual streaks in fiddler crabs. J. Exp. Biol. 223 (1), jeb210195. https://doi.org/10.1242/jeb.210195.

Baird, H.P., Miller, K.J., Stark, J.S., 2011. Evidence of hidden biodiversity, ongoing speciation and diverse patterns of genetic structure in giant Antarctic amphipods. Mol. Ecol. 20 (16), 3439–3454. https://doi.org/10.1111/j.1365-294X.2011.05173.x.

Baldwin Fergus, J.L., Johnsen, S., Osborn, K.J., 2015. A unique apposition compound eye in the mesopelagic hyperiid amphipod *Paraphronima gracilis*. Curr. Biol. 25 (4), 473–478. https://doi.org/10.1016/j.cub.2014.12.010.

Blaxter, M.L., De Ley, P., Garey, J.R., Liu, L.X., Scheldeman, P., Vierstraete, A., Vanfleteren, J.R., Mackey, L.Y., Dorris, M., Frisse, L.M., Vida, J.T., Thomas, W.K., 1998. A molecular evolutionary framework for the phylum Nematoda. Nature 392 (6671), 71–75. https://doi.org/10.1038/32160.

Bovallius, C., 1885. On some forgotten genera among the amphipodous Crustacea. K. - Sven. Vetenskapsakademiens Handl. 10 (14), 1–17.

Bovallius, C., 1887. Systematical list of the Amphipoda Hyperiidea. K. - Sven. Vetenskapsakademiens Handl. 11 (16), 1–50.

Bovallius, C., 1889. Contribution to a monograph of the Amphipoda Hyperiidea. Part I: 2. The families cyllopodidae, paraphronimidae, thaumatopsidae, mimonectidae, hyperiidae, phronimidae, anchylomeridae. K. - Sven. Vetenskapsakademiens Handl. 22 (7), 1–434.

Bowman, T.E., Gruner, H.E., 1973. The families and genera of Hyperiidea (Crustacea: Amphipoda). Smithsonian Contrib. Zool. 146, 1–64. https://doi.org/10.5479/si.00810282.146.

Brown, R.P., Yang, Z., 2011. Rate variation and estimation of divergence times using strict and relaxed clocks. BMC Evol. Biol. 11 (271) https://doi.org/10.1186/1471-2148-11-271.

Browne, W.E., Haddock, S.H., Martindale, M.Q., 2007. Phylogenetic analysis of lineage relationships among hyperiid amphipods as revealed by examination of the mitochondrial gene, cytochrome oxidase I (COI). Integr. Comp. Biol. 47 (6), 815–830. https://doi.org/10.1093/icb/icm093.

Brusca, G.J., 1967. The ecology of pelagic Amphipoda, I. Species accounts, vertical zonation and migration of Amphipoda from the waters off Southern California. Pac. Sci. 21 (3), 382–393.

Burridge, A.K., Tump, M., Vonk, R., Goetze, E., Peijnenburg, K.T.C.A., 2017. Diversity and distribution of hyperiid amphipods along a latitudinal transect in the Atlantic Ocean. Prog. Oceanogr. 158, 224–235. https://doi.org/10.1016/j.pocean.2016.08.003.

Claus, C., 1879. Der organismus der Phronimiden. Arbeiten aus dem Zoologischen Institut der Universität zu Wien 2 (1), 59–146.

Copilaş-Ciocianu, D., Borko, Š., Fišer, C., 2020. The late blooming amphipods: global change promoted post-Jurassic ecological radiation despite Palaeozoic origin. Mol. Phylogenet. Evol. 143, 106664. https://doi.org/10.1016/j.ympev.2019.106664.

Darriba, D., Taboada, G.L., Doallo, R., Posada, D., 2012. jModelTest 2: more models, new heuristics and parallel computing. Nat. Methods 9 (8). https://doi.org/10.1038/nmeth.2109, 772-772.

Drummond, A.J., Suchard, M.A., Xie, D., Rambaut, A., 2012. Bayesian phylogenetics with BEAUti and the BEAST 1.7. Mol. Biol. Evol. 29 (8), 1969–1973. https://doi.org/10.1093/molbev/mss075.

Ezard, T., Fujisawa, T., Barraclough, T.G., 2009. splits: Species' limits by threshold statistics. Available at: URL. https://r-forge.r-project.org/projects/splits/.

Fontaneto, D., Flot, J.-F., Tang, C.Q., 2015. Guidelines for DNA taxonomy, with a focus on the meiofauna. Mar. Biodivers. 45 (3), 433–451. https://doi.org/10.1007/s12526-015-0319-7.

France, S.C., Kocher, T.D., 1996. Geographic and bathymetric patterns of mitochondrial 16S rRNA sequence divergence among deep-sea amphipods, *Eurythenes gryllus*. Marine Biology : International Journal on Life in Oceans and Coastal Waters 126 (4), 633–643. https://doi.org/10.1007/BF00351330.

Fujisawa, T., Barraclough, T.G., 2013. Delimiting species using single-locus data and the generalized mixed yule coalescent approach: a revised method and evaluation on simulated data sets. Syst. Biol. 62 (5), 707–724. https://doi.org/10.1093/sysbio/syt033.

Gasca, R., Hoover, R., Haddock, S.H.D., 2015. New symbiotic associations of hyperiid amphipods (Peracarida) with gelatinous zooplankton in deep waters off California. J. Mar. Biol. Assoc. U. K. 95 (3), 503–511. https://doi.org/10.1017/S0025315414001416.

Geller, J., Meyer, C., Parker, M., Hawk, H., 2013. Redesign of PCR primers for mitochondrial cytochrome c oxidase subunit I for marine invertebrates and application in all-taxa biotic surveys. Molecular Ecology Resources 13 (5), 851–861. https://doi.org/10.1111/1755-0998.12138.

Geomar Helmholtz-Zentrum für Ozeanforschung, Hissmann, K., Schauer, J., 2017. Manned submersible JAGO. Journal of large-scale research facilities 3, 1–12. https://doi.org/10.17815/jlsrf-3-157.

Gilly, W.F., Beman, J.M., Litvin, S.Y., Robison, B.H., 2013. Oceanographic and biological effects of shoaling of the oxygen minimum Zone. Annual Review of Marine Science 5 (1), 393–420. https://doi.org/10.1146/annurev-marine-120710-100849.

Guérin-Méneville, F.E., 1836. Iconographie du règne animal de G. Cuvier; ou, Représentation dáprès nature de lúne des espèces les plus remarquables, et souvent non encore figurées, de chaque genre dánimaux. Avec un texte descriptif mis au courant de la science. Ouvrage pouvant servir d'atlas à tous les traités de zoologie. 6. Crustacés. J. B. Baillière, Paris.

Hallberg, E., Skog, M., 2011. Chemosensory sensilla in crustaceans. In: Breithaupt, T., Thiel, M. (Eds.), Chemical Communication in Crustaceans. New York, NY: Springer, New York, pp. 103–121.

Harbison, G.R., 1998. The parasites and predators of Thaliacea. In: Bone, Q. (Ed.), The Biology of Pelagic Tunicates. Oxford University Press, Oxford, pp. 186–214.

Harbison, G.R., Biggs, D.C., Madin, L.P., 1977. The associations of Amphipoda Hyperiidea with gelatinous zooplankton—II. Associations with Cnidaria, Ctenophora and Radiolaria. Deep Sea Research 24 (5), 465–488. https://doi.org/10.1016/0146-6291(77)90484-2.

Hoving, H.-J.T., Hauss, H., Schütte, F., Merten, V., Fabrizius, E., Hissmann, K., Schauer, J., Striewski, P., Vereira, N., Robison, B.H., Osborn, K., 2018. Cruise Report POS520 RV POSEIDON Mindelo, Cape Verde (14/2/2018) – Mindelo Cape Verde (1/3/2018) Biological baseline studies in the pelagic deep seas of Cape Verde. Retrieved from Kiel, Germany. http://oceanrep.geomar.de/44423/.

Hoving, H.-J.T., Hauss, H., Freitas, R., Hissmann, K., Osborn, K., Scheer, S.L., Merten, V., Hans, A.C., 2019. The role of gelatinous macrozooplankton in deep-sea carbon transport in Cape Verde Cruise No. POS532. Retrieved from Kiel, Germany. http://oceanrep.geomar.de/50197/.

Hurt, C., Haddock, S.H.D., Browne, W.E., 2013. Molecular phylogenetic evidence for the reorganization of the Hyperiid amphipods, a diverse group of pelagic crustaceans. Mol. Phylogenet. Evol. 67 (1), 28–37. https://doi.org/10.1016/j.ympev.2012.12.021.

International Commission on Zoological Nomenclature, 1997. Opinion 1878. *Paraphronima crassipes* Claus, 1879 (Crustacea, Amphipoda): specific name conserved. Bull. Zool. Nomencl. 54 (3), 194.

Kapli, P., Lutteropp, S., Zhang, J., Kobert, K., Pavlidis, P., Stamatakis, A., Flouri, T., 2017. Multi-rate Poisson tree processes for single-locus species delimitation under maximum likelihood and Markov chain Monte Carlo. Bioinformatics 33 (11), 1630–1638. https://doi.org/10.1093/bioinformatics/btx025.

Katoh, K., Standley, D.M., 2013. MAFFT multiple sequence alignment software version 7: improvements in performance and usability. Mol. Biol. Evol. 30 (4), 772–780. https://doi.org/10.1093/molbev/mst010.

Knowlton, N., 1993. Sibling species in the sea. Annu. Rev. Ecol. Systemat. 24 (1), 189–216. https://doi.org/10.1146/annurev.es.24.110193.001201.

Knowlton, N., 2000. Molecular genetic analyses of species boundaries in the sea. Hydrobiologia 420 (1), 73–90. https://doi.org/10.1023/A:1003933603879.

Kumar, S., Stecher, G., Li, M., Knyaz, C., Tamura, K., 2018. Mega X: molecular evolutionary genetics analysis across computing platforms. Mol. Biol. Evol. 35 (6), 1547–1549. https://doi.org/10.1093/molbev/msy096.

Land, M.F., 1989. The eyes of hyperiid amphipods: relations of optical structure to depth. J. Comp. Physiol. A Sens. Neural Behav. Physiol. 164 (6), 751–762. https://doi.org/10.1007/BF00616747.

Land, M.F., 2000. On the functions of double eyes in midwater animals. Phil. Trans.: Biol. Sci. 355 (1401), 1147–1150.

Laval, P., 1980. Hyperiid amphipods as crustacean parasitoids associated with gelatinous zooplankton. Oceanogr. Mar. Biol. Annu. Rev. 18, 11–56.

Lavaniegos, B., Ohman, M.D., 1999. Hyperiid amphipods as indicators of climate change in the California Current. In: Schram, F.R., von Vaupel Klein, J.C. (Eds.), Crustaceans and the Biodiversity Crisis: Proceedings of the Fourth International Crustacean Congress. Brill, Amsterdam, The Netherlands, pp. 489–509.

Lo Bianco, S., 1909. Notizie biologiche riguardanti specialmente il periodo di maturita sessuale degli animali del golfo di Napoli. Mittheilungen aus der Zoologischen Station zu Neapel 19, 513–761.

Madin, L.P., Harbison, G.R., 1977. The associations of Amphipoda Hyperiidea with gelatinous zooplankton—I. Associations with Salpidae. Deep Sea Research 24 (5), 449–463. https://doi.org/10.1016/0146-6291(77)90483-0.

Meyer-Rochow, V.B., 1978. The eyes of mesopelagic crustaceans. II. *Streetsia challengeri* (amphipoda). Cell Tissue Res. 186 (2), 337–349. https://doi.org/10.1007/bf00225542.

Meyer-Rochow, V.B., 2015. Compound eyes of insects and crustaceans: some examples that show there is still a lot of work left to be done. Insect Sci. 22 (3), 461–481. https://doi.org/10.1111/1744-7917.12117.

Miller, M.A., Pfeiffer, W., Schwartz, T., 2010. 14-14 Nov. 2010. Creating the CIPRES Science Gateway for inference of large phylogenetic trees. In: Paper Presented at the 2010 Gateway Computing Environments Workshop (GCE).

Norris, R.D., 2000. Pelagic species diversity, biogeography, and evolution. Paleobiology 26 (4), 236–258.

Palumbi, S.R., 1994. Genetic divergence, reproductive isolation, and marine speciation. Annu. Rev. Ecol. Systemat. 25 (1), 547–572. https://doi.org/10.1146/annurev.es.25.110194.002555.

Palumbi, S.R., 1996. Nucleic acids II: the polymerase chain reaction. In: Hillis, D.M., Moritz, C., Mable, B.K. (Eds.), Molecular Systematics, second ed. Sinauer Associates Inc, Sunderland, pp. 205–247.

Pilar Cabezas, M., Cabezas, P., Machordom, A., Guerra-García, J.M., 2013. Hidden diversity and cryptic speciation refute cosmopolitan distribution in *Caprella penantis* (Crustacea: Amphipoda: caprellidae). J. Zool. Syst. Evol. Res. 51 (2), 85–99. https://doi.org/10.1111/jzs.12010.

Pinnegar, J.K., Goñi, N., Trenkel, V.M., Arrizabalaga, H., Melle, W., Keating, J., Óskarsson, G., 2015. A new compilation of stomach content data for commercially important pelagic fish species in the northeast Atlantic. Earth Syst. Sci. Data 7 (1), 19–28. https://doi.org/10.5194/essd-7-19-2015.

Puillandre, N., Lambert, A., Brouillet, S., Achaz, G., 2012. ABGD, automatic barcode gap discovery for primary species delimitation. Mol. Ecol. 21 (8), 1864–1877. https://doi.org/10.1111/j.1365-294X.2011.05239.x.

R Core Team, 2017. R: A Language and Environment for Statistical Computing. R Foundation for Statistical Computing, Vienna, Austria. Retrieved from. https://www.R-project.org.

Rambaut, A., Drummond, A.J., Xie, D., Baele, G., Suchard, M.A., 2018. Posterior summarization in Bayesian phylogenetics using Tracer 1.7. Syst. Biol. 67 (5), 901–904. https://doi.org/10.1093/sysbio/syy032.

Robison, B.H., 2004. Deep pelagic biology. J. Exp. Mar. Biol. Ecol. 300 (1), 253–272. https://doi.org/10.1016/j.jembe.2004.01.012.

Robison, B.H., 2009. Conservation of deep pelagic biodiversity. Conserv. Biol. 23 (4), 847–858.

Ronquist, F., Teslenko, M., van der Mark, P., Ayres, D.L., Darling, A., Höhna, S., Larget, B., Liu, L., Suchard, M.A., Huelsenbeck, J.P., 2012. MrBayes 3.2: efficient Bayesian phylogenetic inference and model choice across a large model space. Syst. Biol. 61 (3), 539–542. https://doi.org/10.1093/sysbio/sys029.

Smith-Beasley, L., 1992. *A study of the vertical distribution of upper mesopelagic animals in the Monterey Submarine Canyon, California.* (Master of Science), San Jose State University, Stamatakis, A. 2014. RAxML version 8: a tool for phylogenetic analysis and post-analysis of large phylogenies. Bioinformatics 30 (9), 1312–1313. https://doi.org/10.1093/bioinformatics/btu033.

Stebbing, T.R.R., 1888. Report on the Amphipoda collected by H.M.S. *Challenger* during the years 1873-1876. *Report on the Scientific Results of the Voyage of H.M.S. Challenger during the years 1873–76*. Zoology 29 i-xxiv + 1-1737.

Tang, C.Q., Humphreys, A.M., Fontaneto, D., Barraclough, T.G., 2014. Effects of phylogenetic reconstruction method on the robustness of species delimitation using single-locus data. Methods in Ecology and Evolution 5 (10), 1086–1094. https://doi.org/10.1111/2041-210x.12246.

Tempestini, A., Fortier, L., Pinchuk, A., Dufresne, F., 2017. Molecular phylogeny of the genus *Themisto* (Guérin, 1925) (Amphipoda: hyperiidae) in the northern hemisphere. J. Crustac Biol. 37 (6), 732–742. https://doi.org/10.1093/jcbiol/rux076.

Thurston, M.H., 1976. The vertical distribution and diurnal migration of the Crustacea Amphipoda collected during the SOND Cruise, 1965 II. The Hyperiidea and general discussion. J. Mar. Biol. Assoc. U. K. 56 (2), 383–470. https://doi.org/10.1017/S0025315400018981.

Vinogradov, M.E., Volkov, A.F., Semenova, T.N., 1996. In: Siegel-Causey, D. (Ed.), Hyperiid Amphipods (Amphipoda, Hyperiidea) of the World Oceans. Science Publishers, Inc, Lebanon, USA.

Westram, A.M., Jokela, J., Keller, I., 2013. Hidden biodiversity in an ecologically important freshwater amphipod: differences in genetic structure between two cryptic species. PloS One 8 (8), e69576. https://doi.org/10.1371/journal.pone.0069576.

Widder, E., 2002. Bioluminescence and the pelagic visual environment. Mar. Freshw. Behav. Physiol. 35, 1–26. https://doi.org/10.1080/10236240290025581.

Zeidler, W., 1995. Case 2952. *Paraphronima crassipes* Claus, 1879 (Crustacea, Amphipoda): proposed conservation of the specific name. Bull. Zool. Nomencl. 52 (4), 310–312.

Zeidler, W., 2003. A review of the hyperiidean amphipod superfamily Vibilioidea Bowman and Gruner, 1973 (Crustacea: Amphipoda: Hyperiidea). Zootaxa 280 (1), 1–104. https://doi.org/10.11646/zootaxa.280.1.1.

Zeidler, W., Browne, W.E., 2015. A new *Glossocephalus* (Crustacea: Amphipoda: Hyperiidea: Oxycephalidae) from deep-water in the Monterey Bay region, California, USA, with an overview of the genus. Zootaxa 4027 (3), 408–424. https://doi.org/10.11646/zootaxa.4027.3.5.

Zeil, J., 1983. Sexual dimorphism in the visual system of flies: the compound eyes and neural superposition in bibionidae (Diptera). J. Comp. Physiol. 150 (3), 379–393. https://doi.org/10.1007/BF00605027.

Zhang, J., Kapli, P., Pavlidis, P., Stamatakis, A., 2013. A general species delimitation method with applications to phylogenetic placements. Bioinformatics 29 (22), 2869–2876. https://doi.org/10.1093/bioinformatics/btt499.